Journal of Low Temperature Physics, Vol. 143, Nos. 3/4, May 2006 (© 2006)
DOI: 10.1007/s10909-006-9211-y

^{2}H-Solid State NMR Studies of Tunneling Phenomena and Isotope Effects in Transition Metal Dihydrides

Gerd Buntkowsky[1] and Hans-Heinrich Limbach[2]

[1] *Department of Physical Chemistry, FSU Jena, Helmholtzweg 4, Jena, D-07743, Germany*
E-mail: gerd.buntkowsky@uni-jena.de
[2] *Department of Physical Chemistry, FU Berlin, Takustr. 3, D-14195, Berlin, Germany*

(Received March 24, 2005; revised October 10, 2005)

In many transition metal dihydrides and dihydrogen complexes the hydrogens are relatively weakly bound and exhibit a fairly high mobility, in particular with respect to their mutual exchange. Part of this high mobility is due to the exchange symmetry of the two hydrogens, which causes an energy splitting into even and odd spatial energy eigenfunctions, resulting in the typical coherent tunneling of a two-level system. Owing to the quantum mechanical symmetry selection principles the eigenfunctions are connected to the possible nuclear spin states of the system. If the tunneling frequency is in the proper frequency window it is thus possible to observe these tunneling transitions by NMR at very low temperatures, where no thermally induced exchange reactions overshadow the tunneling. The first part of this review gives an introduction into the interplay of chemical kinetics and tunneling phenomena in general, rotational tunneling of dihydrogen in a two-fold potential in particular and the Bell tunnel model, followed by a summary of solid state NMR techniques for the observation of these tunnel processes. Then a discussion of the effects of these processes on the ^2H NMR line shape is given. The second part of the review reports results of a ^2H-solid state NMR spectroscopy and T_1 relaxatiometry study of trans-$[Ru(D_2)Cl(PPh_2CH_2CH_2PPh_2)_2]PF_6$, in the temperature regime from 5.4 to 320 K. In the Ru-D_2 sample coherent tunneling and incoherent exchange processes on the time scale of the quadrupolar interaction are observed. From the spectra and T_1-data the height of the tunneling barrier is determined. Next results of ^2H-spin–lattice relaxation measurements for a selectively $\eta^2 - D_2$ labeled isotopomer of the complex $W(PCy_3)_2(CO)_3)(\eta^2 - D_2)$ are presented and discussed. The relaxation measurements are analyzed in terms of a simple one dimensional Bell tunnel model and comparison to incoherent neutron scattering (INS) data from the H_2 complex. The comparison reveals a strong isotope effect of 2×10^3 for the exchange rates of the deuterons versus hydrons.

KEY WORDS: Solid state NMR; tunneling; quantum coupling; dihydrogen complex; 2H-NMR; dipolar interactions; quadrupoler interactions.

Table of Contents

1. INTRODUCTION

Non-classical transition metal hydrides with η^2-bonded dihydrogen ligands have very interesting physical, spectroscopic and chemical properties and are attracting much experimental and theoretical interest.[1–21] Following the pioneering work of Kubas *et al.*[22,23] a whole series of transition metal polyhydrides with hydrogen distances varying between 0.8 and 1.7 Å were synthesized.[20,24–28] Understanding their chemistry has led to a better understanding of catalysis since they may be catalytic precursors or stable models for short lived intermediate steps in catalysis[12,29–31] and are of current interest in organometallic chemistry.[32–35]

In these compounds the hydrogen atoms are not fixed in space as in conventional hydrogen bonds, but exhibit a rather high mobility. In particular they can exchange their positions, either at higher temperatures due to conventional chemical exchange or at low temperatures due to quantum mechanical tunneling. The mutual exchange of the hydrons (i.e. ^{1}H, ^{2}H or ^{3}H) is equivalent to a hindered 180° rotation around the axis intersecting the M-H_2 angle.[36–40] The rotational barrier is caused mainly by the chemical structure involving the binding of the hydrons to the metal, effects of the ligands and sometimes also by crystal effects from neighboring molecules. The two-fold symmetry of the barrier causes a splitting of the energy eigenstates into states with even and odd symmetry (see Fig. 1). For identical hydrogen isotopes, the quantum mechanical symmetry principles have to be fulfilled, leading for spin 1/2 particle to the formation of *para*-states with anti parallel and *ortho*-states with parallel nuclear spins. For isotope mixtures like HD, no such symmetry principles exist. The height of the barrier determines the energy difference between the lowest even and odd symmetry, the so-called tunnel splitting, which can be expressed as a tunnel frequency ν_t. This tunnel splitting depends very strongly on the hindering potential, varying from 10^{12} Hz for dihydrogen gas to a few Hz as the depth of the potential is increased. Due to this large range of tunnel frequencies no single spectroscopic technique is able to cover the whole dynamic range. While fast coherent tunneling in the frequency range of

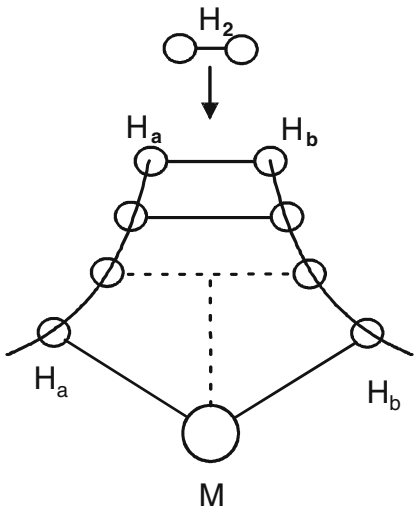

Fig. 1. Sketch of a hydrogen molecule binding to a transition metal: When the H_2 or D_2 molecule is bound to a transition metal, different states are passed, ranging from the free hydrogen molecule over various dihydrogen states to the strongly bound dihydride. These states can be characterized by their R_{HH} or R_{MH} distance as reaction coordinate.

GHz to THz were studied by incoherent neutron scattering (INS),[16,41] relatively slow tunneling processes in the frequency range of (Hz to kHz) are investigated by ^{1}H-liquid state NMR spectroscopy (see for example Refs. 16,42–48 and many others) or ^{2}H-liquid state NMR.[49] In these ^{1}H-liquid state NMR studies the tunnel frequency is usually termed "quantum exchange coupling", due to the fact that the effect of the tunneling on the ^{1}H-liquid state NMR spectra is equivalent to the effect of an indirect spin coupling (J-coupling).

Superimposed on the coherent exchange are incoherent exchange processes, which were also observed in the NMR spectra of these hydrides. In the case of a HD pair, these incoherent processes correspond to H/D scrambling between the two different molecular sites in which the pair is located. In contrast to the quantum exchange, the incoherent exchange leads to a magnetic equivalence of the coupled hydrogen nuclei, i.e., to line broadening and coalescence. This process also leads to characteristic line shape changes in INS spectra[16] and affects the results of *para*-H_2 induced nuclear spin polarization experiments.[50] These line shape changes can be described quantitatively in terms of the quantum-mechanical density matrix formalism developed by Alexander[51] and Binsch[52,53] where only the nuclear spin degrees of freedom are treated quantum-mechanically and the spatial degrees of freedom (bath coordinates) are treated via phenomenological rate

constants. Theoretical interpretations of these rate constants are given by Szymanski[54,55] and Scheurer *et al.*[56,57] The advantage of the Alexander–Binsch formalism is that it is directly comparable to the NMR experiment, because NMR measures the projection of the molecular system onto the spin system. Thus a more detailed theory in the future only needs to reproduce these rate constants, but not the NMR spectra from which these constants were extracted. Finally we wish to note that field cycling NMR studies are an alternative way for the study of these tunnel processes,[58–66] which are however beyond the scope of this review.

The dynamic range of NMR spectroscopy for the study of these tunnel processes is limited by the size of the typical frequency differences of the NMR method used. For the line shape analysis of ^{1}H NMR spectra this means that for a typical spectrometer a range of less than $\approx$10 kHz is accessible in liquids. In principle this range could be increased by ^{1}H-solid state NMR measurements. In practice however, to the best of our knowledge, the strong homonuclear dipolar interactions of the protons have rendered all such attempts unsuccessful. Pairs of deuterons are the only other stable nuclei, where these effects can be observed. Since the chemical shift range of deuterons is limited to $\approx$1.4 kHz only very slow tunnel processes are in principle directly observable in ^{2}H NMR spectroscopy. In liquids faster tunnel processes could only be observable via relaxation measurements. The situation is different in the solid state. Since deuterons are quadrupolar nuclei, they exhibit electric quadrupolar interactions which are typically on the order of 100 kHz in the solid state. For non-oriented samples they give rise to the well-known line shape features in solid state ^{2}H NMR spectra.[67] The quadrupolar interaction reflects the symmetry of the electric field gradient tensor at the position of the nucleus studied and is a very efficient measure of its electronic binding characteristics. Changes in the orientation of the quadrupolar tensor with respect to the external magnetic field are a very sensitive probe for any type of nuclear motion inside the sample. Due to this fact, besides numerous studies of incoherent motions (see for example Refs. 68,69 or the text book[70]), there are also several studies where coherent ^{2}H motions were observed in methyl groups[70–74] and in fact methyl group tunneling seems to be quite a common phenomenon at low temperatures[75–80] as is ammonium tunneling.[81–83] In solid dideuterium systems, however, until now only one example exists where coherent rotational tunneling was observed in the solid state.[39] The main reason for this is that it is no trivial task to find a suitable system for the study of tunneling by ^{2}H NMR, because not only must the height of the rotational barrier must be in the experimentally accessible range, it is also necessary that a stable selective deuteration of the η^2-bound hydrogen positions can be achieved.

In the present review we present results from ^2H low temperature solid state NMR spectroscopy of solid η^2-bound transition metal dihydrogen complexes. These transition metal complexes are model compounds for the various transient states a hydrogen molecule passes through in a catalytic or enzymatic reaction. In the course of this reaction the intermediate states are in general not accessible by NMR spectroscopy, due to their short lived nature. In the η^2-bound transition metal complex, however, the dihydrogen complex state is "frozen", i.e. the distances between the hydrogen and the metal and between the two hydrogen atoms are fixed and it is possible to study the structure and dynamics in this state with NMR spectroscopy. The characterization of the structure and dynamics of these tunneling systems is a very interesting spectroscopic task.

This review is divided as follows: after this introduction, a short survey of quantum mechanical tunneling is given. Then the effects of tunneling on chemical kinetics are summarized. Finally, isotope effects on kinetic processes are discussed. The next section, which is written in the style of a short solid state NMR textbook, summarizes the mathematical and technical tools necessary for understanding the results parts of the work. After the introduction of the basic spin Hamiltonians and the dynamics of spin-wave functions in Hilbert space, the orientation dependence of the spin interactions are discussed, followed by a short introduction to magic angle spinning (MAS) and simple line shape analysis of powder spectra of non-oriented samples. The final part of this section gives a Liouville space representation of the description of dynamic processes and chemical kinetics, followed by an Alexander–Binsch type representation of the NMR theory of a coupled deuterium pair under the influence of coherent tunneling and incoherent exchange and numerical results of this theory.

Next the experimental section follows. First an overview of the investigated samples is given. Then the studies of the rotational dynamics of η^2-bound transition metal dideuterides by means of low temperature ^2H-solid state NMR spectroscopy and relaxometry are reported. Two different systems are investigated in this part: a Ru-D_2 complex with a relatively high rotational barrier and a W-D_2 complex with a lower rotational barrier. In the Ru-D_2 system experimental evidence for coherent D_2 tunneling is found. The tunnel splitting and height of the tunnel barrier are elucidated and the strongly non-classical dynamics of the dideuteron pair is analyzed in detail in the temperature range from 5.2 up to 300 K. In the W-D_2 system also a non-classical dynamical behavior of the deuteron exchange is observed in the spin–lattice relaxation data. This again indicates a quantum mechanical tunneling of the deuterons. From the temperature dependence of the rates the height of the rotational barrier is estimated. The comparison of the resulting data to INS data obtained

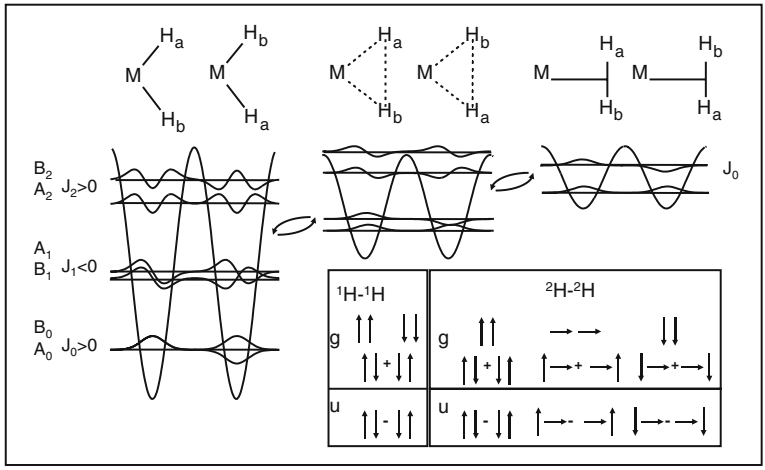

Fig. 2. Sketch of the energy eigenstates of a dihydrogen H_a–H_b system in a two fold rotational potential and symbolic representation of the symmetry adapted spin eigenfunctions. The spatial eigenstates are labeled A_k and according to the irreducible representation of the C_2 group. The spin functions are labeled as g (gerade) for the even and u (ungerade) for the odd linear combinations. The tunnel splitting is the energy difference between adjacent levels $J_k = E(B_k) - E(A_k)$. For a pair of identical hydrogen isotopes the whole wave function has to be either antisymmetric (^{1}H–^{1}H, fermionic system) or symmetric (^{2}H–^{2}H, bosonic system). Thus for an ^{1}H–^{1}H pair, the spatial A_k and B_k functions couple to the u and g spin functions, respectively, and for an ^{2}H–^{2}H pair, the spatial A_k and B_k functions couple to the g and u spin functions, respectively. Upon transitions between the dihydride (leftmost potential) to the strongly and weakly bound dihydrogen states (center and right potential) the depth of the hindering potential decreases and the tunnel splitting increases.

on the protonated complex reveals an unexpectedly strong ^{1}H–^{2}H isotope effect (Fig. 2).

2. TUNNELING AND CHEMICAL KINETICS

This section gives an introduction to the effects of quantum mechanical tunneling on chemical reactions. The first part describes the basic properties of coherent rotational tunneling, the next section reviews incoherent tunneling and the Bell tunnel model and the last section discusses briefly the appearance of isotope effects in tunneling systems.

2.1. Coherent Rotational Tunneling

In different parts of science there are several incongruent definitions of coherent and incoherent tunneling or exchange, mainly out of histor-

ical or practical reasons. In the following the definition most amenable to NMR spectroscopy is used, i.e.: an exchange process of a particle is called coherent, if the motion is related to a splitting of energy levels and the probability of finding the particle in a given state changes periodically (modulo some phase relaxation time) as a function of time; if however external bath degrees of freedom are involved in the dynamics of the system or the probability is describable as a rate process approaching an equilibrium, the process is called incoherent.

Coherent rotational tunneling is similar to the quantum mechanical tunneling of a particle in a symmetric double minimum potential. The symmetry of the potential causes a splitting of the ground state into a doublet, where the energy levels are separated by the tunnel frequency.[84] Since the exchange of the two hydrogen isotopes is a symmetry operation, the corresponding hindering potential possesses an exact two-fold symmetry.

The basic principles of the coherent rotational tunneling in transition metal dihydrides can be most easily discussed using the model of a one dimensional hindered quantum mechanical rotor. In this model it is assumed that the distance between the two hydrons, as well as their distance from the metal, does not change. In this case the angular position, described via an angle φ, is used as a degree of freedom. The corresponding Schrödinger equation of a rigid rotor in a harmonic twofold potential is expressed as ($2V_0$ describes the depth of the hindering potential):

$$-\frac{\hbar^2}{2mr^2}\frac{d^2}{d\varphi^2}|\Psi\rangle - V_0(1-\cos 2\varphi)|\Psi\rangle = E|\Psi\rangle \tag{1}$$

This is a Matthieu type differential equation. It has well known solutions with the following properties: Due to the C_2 symmetry of the problem, the resulting eigenstates have either even or odd symmetry and the whole Hilbert space splits up into an odd and an even subspace. The corresponding eigenfunctions can be easily calculated numerically by expanding Eq. (1) into a matrix eigenvalue problem using appropriately normalized sine (for the odd subspace) and cosine functions (for the even subspace) as base functions. The resulting eigenfunctions in these two sets are cosine type functions $C_n(\varphi)$, which are a superposition of the cosine functions and sine type functions $S_n(\varphi)$, which are a superposition of the sine functions (Fig. 3). The ground state wave function is always a cosine type state with even symmetry and the first excited state is always a sine type function with odd symmetry.

The energy differences between different $C_n(\varphi)$ or $S_n(\varphi)$ depends strongly on the depth of the potential $2V_0$ and varies between zero and the order of typical rotational μ-wave or IR transitions (Fig. 4). At temperatures in the range of 10 K only the lowest pair of eigenstates is thermally populated. If both hydrons are identical (i.e. both are ^{1}H or ^{2}H),

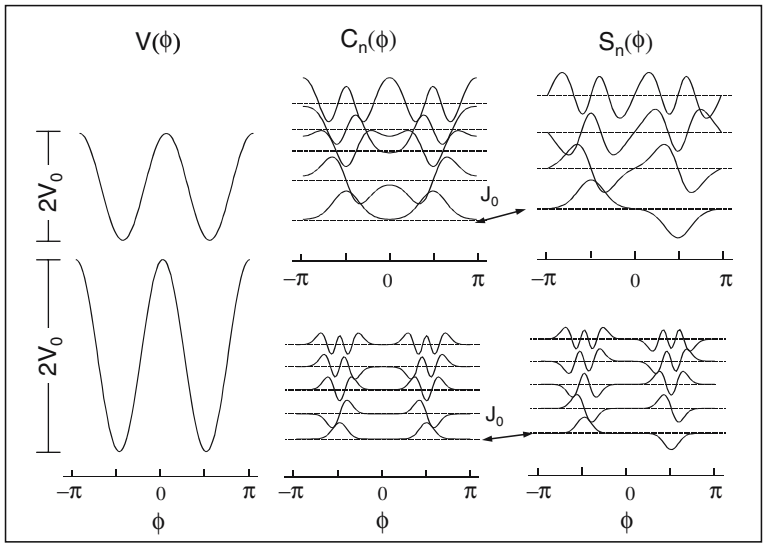

Fig. 3. Sketch of eigenstates and energy eigenvalues of the Schrödinger equation of a rigid D_2 rotor in a harmonic twofold potential for two different depths of the potential barrier. Upper panel: $V_0 = 10^7$ MHz, $J_0 = 6.4 \times 10^3$ MHz, lower panel: $V_0 = 10^8$ MHz, $J_0 = 60$ Hz. Left: Potential energy curve $V(\phi)$, middle panel: Cosine type eigenfunctions $C_n(\phi)$, right panels: Sine type eigenfunctions $S_n(\phi)$. The energy shift between cosine and sine functions is increased artificially to demonstrate the differences in J_n between energy levels of same n.

the Pauli exclusion principle has to be fulfilled. The implications are discussed in detail in Ref. 85. From this it follows, that the spatial states are connected to spin states in such a way that the whole wave function is either anti-symmetric (for ^{1}H) or symmetric (for ^{2}H). Due to this correlation of spin and spatial state, the energy difference ΔE between the lowest two spatial eigenstates can be seen as an exchange coupling J_0 in NMR spectroscopy, similar to the Dirac exchange interaction of electronic spins. As a result a spin tunnel Hamiltonian, which describes the splitting between adjacent states of different symmetry, can be defined. If the tunnel splitting is of the magnitude of interactions in the NMR spectrum, it is directly visible in the NMR spectrum.

If several pairs of tunnel levels are thermally populated, the thermal average of the different pairs of tunnel levels has to be calculated. As long as only a few levels far below the barrier are contributing, the values of the various tunnel frequencies $J_n = \nu_{\text{tn}}$ will be small compared to the thermal exchange rates between the level pairs and the averaging can be done by summing up the individual values of ν_{tn}, times their thermal popula-

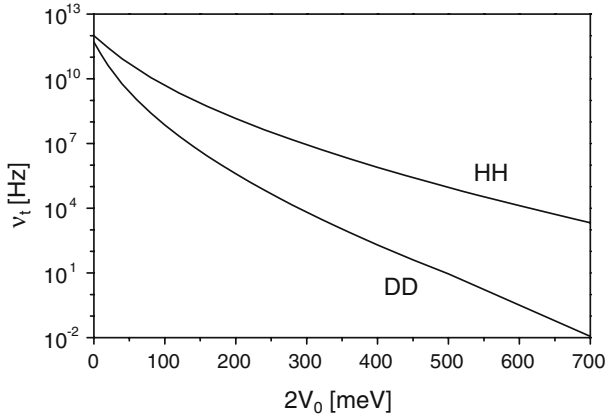

Fig. 4. Tunnel frequency and HH/DD isotope effect as a function of the barrier height $2V_0$ for a proton pair HH and a deuteron pair DD with $R_{DD} = 1$ Å.

tion. This averaging can be approximated using the population of one of the connected levels.

$$\nu_t = \sum_n \nu_{tn} \exp\left(-\frac{E_n}{kT}\right) \tag{2}$$

The situation becomes more difficult if the values of ν_t are comparable or greater than the thermal population rates or decay rates. In this regime, a transition from coherent to incoherent exchange will take place, as described in more detail in Ref. 16. There it is shown that it is possible, despite the large range of tunnel frequencies, varying between Hz and THz, to describe the whole dynamic by a single theory: Depending on the size of the tunnel frequency the two hydrons will exhibit strong differences in their dynamic behavior. For a low barrier height, a large tunnel frequency is observed. The dihydrogen pair will be at least partially delocalized and acts more or less like a one-dimensional free quantum mechanical rotor, similar to p-H_2 and o-H_2, allowing coherent (i.e. strictly periodic) exchange processes of the individual hydrons with the tunnel frequency ν_t. For high potential barriers the tunnel splitting goes to zero, no coherent exchange processes take place and each hydron is located in a single potential minimum and the dihydrogen pair is fixed. In this situation for an exchange of the two hydrons to occur a coupling to external degrees of freedom is necessary. In this scenario the exchange of the two hydrogen atoms is describable as a thermally activated rate process. Compared to the previous coherent exchange, the thermally activated rate process corresponds to an incoherent exchange of the two hydrons, which

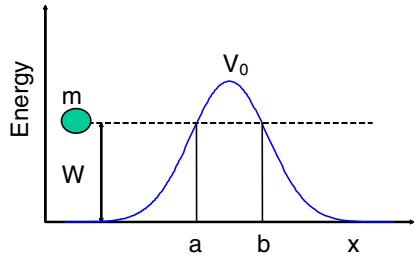

Fig. 5. Tunneling through a energy barrier: While the particle **m** with energy $W < V_0$ is classical reflected at **a**, quantum mechanics allows a tunneling through the barrier from **a** to **b**.

leads to an exponential decaying curve for the probability of finding one hydron at its initial position.

2.2. Incoherent Tunneling and the Bell Model

Parallel to the coherent tunneling due to the splitting of energy levels as discussed in the previous subsection, there is a second type of tunnel processes, describing the classical forbidden penetration of a barrier (Fig. 5).

The probability of penetrating the barrier depends on the energy of the incident particle and the width, shape and height of the potential barrier. For most potentials only approximate solutions (for example WKB approximation[84]) or numerical calculations of the transition probability are possible. Analytically solvable exceptions include rectangular potential steps and parabolic potentials. While the former give only very crude approximations of a real world system, the latter, also known as the Bell tunneling model, gives reasonably good results, when compared to experimentally determined rate constants.

This subsection gives a short review of the Bell tunnel model,[86] which is employed later for describing the temperature dependence of the incoherent exchange processes in the Ru-D_2 sample. The basic idea of the model is to describe the potential barrier as an inverted parabola and use the known solution of the quantum mechanical harmonic oscillator for calculation of the transition probability.

Figure 6a displays the potential and ground state of the harmonic oscillator according to the Schrödinger equation

$$\left[\frac{d^2}{dx^2} + \frac{2m}{\hbar^2}\left(E - \frac{1}{2}m\omega_0^2 x^2\right)\right]|\Psi\rangle = 0 \tag{3}$$

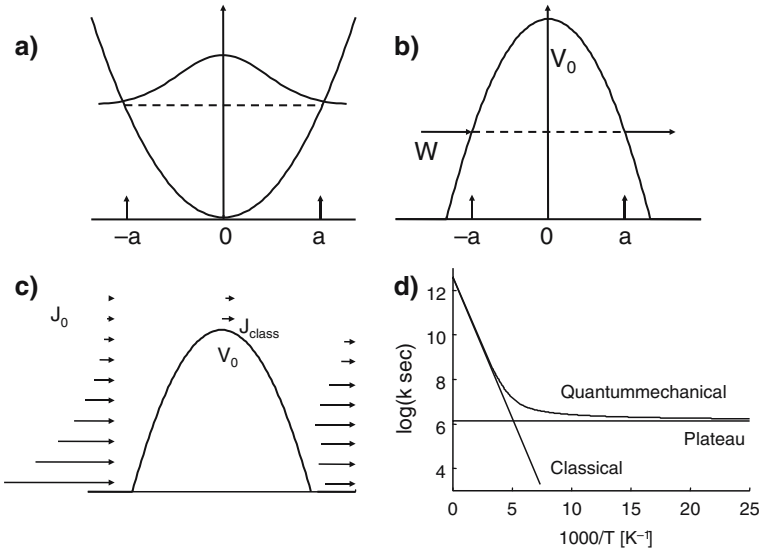

Fig. 6. The Bell Tunnel Model: (a) Quantum mechanical harmonic oscillator with its ground state wave function; (b) Inverted harmonic oscillator potential. (c) a stream of particles with a Boltzmann distribution of energies hits the barrier. Classical only those particles with $W > V_0$ can pass the barrier. Quantum mechanically also particles with $W < V_0$ may pass the barrier. (d) Comparison of classical Arrhenius rate and quantum mechanical corrected rate. While classically the rate goes to zero for $T \to 0$, quantum mechanically a finite plateau is approached.

where the width $2a$ of potential barrier at the ground state energy level is defined through:

$$E_0 = \frac{1}{2}\hbar\omega_0 =: \frac{1}{2}m\omega_0^2 a^2 \tag{4}$$

Solving for $\nu_0 = \omega_0/(2\pi)$ expresses the oscillation frequency via the ground state energy E_0 and the width of the potential at E_0:

$$\nu_0 = \frac{1}{\pi a}\sqrt{\frac{E_0}{2m}} \tag{5}$$

If the oscillator potential is inverted as shown in Fig. 6b,

$$\left[\frac{d^2}{dx^2} + \frac{2m}{\hbar^2}\left(E + \frac{1}{2}m\omega_0^2 x^2\right)\right]|\Psi\rangle = 0 \tag{6}$$

and the previous solution can be reused by introducing the imaginary tunnel frequency ν_t,

$$\nu_t = \frac{1}{\pi a}\sqrt{\frac{E_0}{2m}} \tag{7}$$

which gives the following probability for transition through the barrier:

$$G(W) = \left[1 + \exp\left(\frac{V_0 - W}{h\nu_t}\right)\right]^{-1} \tag{8}$$

In typical chemical reactions a large number of particles N_0 are involved. This situation can be modeled as a stream $J = dN/dt$ of particles hitting the barrier, as sketched in Fig. 6c. If the energy distribution of the particle is described as Boltzmann distribution (dN: number of particles in energy interval $[W, W + dW]$)

$$\begin{aligned} dN &= N_0 \cdot p(W)dW \\ &= N_0 \cdot \frac{1}{kT}\exp\left(-\frac{W}{kT}\right)dW \end{aligned} \tag{9}$$

The stream, i.e. the number of particles per second, which pass the energy barrier, is given as (p(W): probability of energy W; T(W): transition probability at energy W):

$$J = J_0 \int_0^\infty p(W)T(W)dW \tag{10}$$

Classically only those particles with energy $W > V_0$ may pass the barrier,

$$T(W) = \begin{cases} 0 & W \le V_0 \\ 1 & V_0 < W \end{cases} \tag{11}$$

and the classical rate J_c is:

$$J_c = \frac{J_0}{kT}\int_{V_0}^\infty \exp\left(-\frac{W}{kT}\right)dW \tag{12}$$

which after integration yields the Arrhenius law:

$$J_c = J_0 \exp\left(-\frac{V_0}{kT}\right) \tag{13}$$

Quantum mechanically the transition rate J_{QM} of the Bell model is calculated by inserting Eq. (8) into Eq. (10).

$$J_{QM} = \frac{J_0}{kT}\int_0^\infty \exp\left(-\frac{W}{kT}\right) G(W)dW \tag{14}$$
$$= \frac{J_0}{kT}\int_0^\infty \exp\left(-\frac{W}{kT}\right)\left[1+\exp\left(\frac{V_0-W}{h\nu_t}\right)\right]^{-1} dW$$

The tunnel correction finally is defined as the ratio of quantum mechanical to classical rate:

$$Q_t = \frac{J_{QM}}{J_c} = \frac{\exp(V_0/kT)}{kT}\int_0^\infty \exp\left(-\frac{W}{kT}\right) G(W)dW \tag{15}$$

For the numerical evaluation, Eq. (15) can be approximated by replacing the integration with a discrete sum over a set of energy levels. The result of such an evaluation is displayed in Fig. 6d, which compares the classical Arrhenius rate with the quantum mechanical rates calculated from Eq. (14). It is evident that at low temperatures the transition rate reaches a plateau value. This plateau is determined by the tunnel probability at low temperatures. It does not coincide with the tunnel frequency of the coherent tunneling.

2.3. Isotope Effects on Coherent and Incoherent Exchange Processes

This subsection describes the two most important isotope effects on tunneling rates. The first effect results from the mass of the isotope, which stems from the fact that the kinetic energy term in the Schrödinger equation depends on the mass. In the case of coherent tunneling the isotope effect on the tunnel splitting is already included in Fig. 4.

There is a similar mass dependent isotope effect on the incoherent tunnel rate in the Bell model due to the mass dependence of the tunnel frequency ν_t (Eq. (7)). As an example Fig. 7 compares the temperature dependent exchange rates of the various combinations of hydrogen isotopes.

The second isotope effect finally is due to the difference in the zero point energy ΔE of different isotopes, caused by their different masses, which results in different barrier heights of the tunneling barrier (see Fig. 7).

3. SOLID STATE NMR STUDIES OF THE TUNNELING KINETICS

This section gives a summary of the necessary theoretical solid state NMR background of the experiments. The section is divided into several

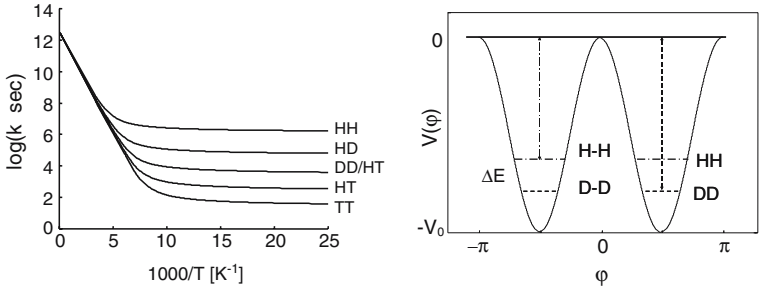

Fig. 7. Left: Mass isotope effects of the different hydrogen isotopes in the Bell model. Right: Isotope effect caused by the zero point energy differences.

parts: first the static NMR interactions, describable by time independent interaction Hamiltonians are introduced, followed by dynamic interactions due to coherent particle exchange. Next the quantum mechanical Hilbert space description of NMR spectroscopy in terms of the solution of the time dependent Schrödinger equation is summarized and finally the full quantum mechanical Liouville formalism of NMR theory, used for the description of the simultaneous presence of coherent and incoherent exchange processes, is supplied. Nuclear Magnetic Resonance (NMR)[87,88] is a spectroscopic technique which covers a very large range of application areas, due to the multitude of different NMR techniques which are available today. Roughly three principal NMR domains can be distinguished, namely liquid state NMR spectroscopy,[89] spatially resolved NMR techniques[90–92] and solid state NMR spectroscopy.[70,93] While the main application of liquid state NMR spectroscopy refers to the area of chemical and biochemical analysis of liquid or soluble compounds, spatially resolved NMR techniques are primarily employed for medical and technical applications. Solid state NMR spectroscopy is devoted to the chemical analysis of insoluble compounds, to the study of electronic structures in conducting systems, and generally to the characterization and investigation of structural and dynamic properties of solid systems.

Solid state NMR spectroscopy allows structural and dynamical studies of molecular conformations in solid environments. As far as the dynamic properties of solid systems are concerned, NMR can cover a very large dynamical range: It is possible to study processes on a time scale of 10^{-12} s (indirect detection of a reaction kinetics) to processes on a time scale of 10^7 s (slow dynamic processes like conformational changes of a molecule or slow chemical reactions) and observe directly or indirectly molecular structures and their transformations on these time scales.

3.1. Spin-Hamiltonians

The basic principles of solid state NMR spectroscopy can be most easily understood by discussing the relevant NMR interactions. Since the energies associated with the spin degrees of freedom are well decoupled from the spatial degrees of freedom, it is sufficient to treat the spin quantum mechanically and use a classic description for the spatial degrees of freedom by introducing the spin-Hamiltonian. Thus all motions except the coherent tunneling are treated classically. In contrast to most other types of spectroscopy NMR has the unique feature, that the full quantum mechanical interaction Hamilton operators (Hamiltonians) of the spin system are usually known. As usual all energies are measured in units of the angular velocity (rad/s), i.e. all energies are divided by $\hbar$.

3.1.1. The Zeeman Interaction

The dominating interaction in a conventional NMR-experiment is the Zeeman interaction between a nuclear spin and an external magnetic field $\vec{B}$. In most NMR experiments the magnetic field $\vec{B}$ consists of a constant homogeneous field $\vec{B}_0 = (0, 0, B_0)$, which by convention is chosen to determine the z-direction of the laboratory frame and a transversal time dependent field $\vec{B}_1 = (B_{1x}(t), B_{1y}(t), 0)$. The corresponding Hamiltonians of the Zeeman interaction are $\hat{H}_0$ and $\hat{H}_1$ respectively, where γ is the gyromagnetic ratio of the spin, i.e.

$$\hat{H}_0 = -\gamma B_0 \hat{I}_z \tag{16}$$

and

$$\hat{H}_1 = -\gamma (B_{1x}(t)\hat{I}_x + B_{1y}(t)\hat{I}_y). \tag{17}$$

3.1.2. The Local Interactions

Apart from the global Zeeman interaction $\hat{H}_0$, which is merely an adjustable experimental parameter, there are the interactions caused by local fields. They are the interesting contributions to the spin Hamilton operator, because only they contain non-trivial information about the system. For organic solids essentially the following contributions are of importance: the dipolar interaction with other nuclear spins $\hat{H}_D$, the screening of the external magnetic field by the electron cloud, i.e. the chemical shift Hamiltonian $\hat{H}_{CS}$, the interaction of a nuclear quadrupolar moment with an electric field gradient, i.e. the quadrupolar interaction $\hat{H}_Q$, the exchange or tunnel interaction $\hat{H}_X$ and finally the indirect

spin–spin-interaction, i.e. the J-coupling $\hat{H}_J$. In addition to these interactions there are several others (for example Knight-Shift, Paramagnetic Shift), which are, however, of no importance in the present context. All these local interactions add to the Zeeman interaction to form the total spin Hamiltonian of the system.

$$\hat{H} = \hat{H}_0 + \hat{H}_1 + \hat{H}_D + \hat{H}_{CS} + H_Q + \hat{H}_X + H_J \tag{18}$$

3.1.3. The High Field Approximation

In most NMR experiments on organic systems the nuclear Zeeman interaction with the static external magnetic field $\vec{B}_0$ is much stronger than all other interactions of the nuclear spins. As a result of these differences in the size, it is usually possible to treat these interactions in first order perturbation theory, i.e. use only those terms which commute with the Zeeman Hamiltonian, the so called secular terms. This approximation is called the high field approximation. While the single particle interactions like CSA or quadrupolar interaction have a unique form, for bilinear interactions, one has to distinguish between a homonuclear and a heteronuclear case, due to the permutation symmetry of identical particles.

3.1.4. The Magnetic Dipolar Interaction

The magnetic dipolar interaction is a result of the classical interaction of two magnetic dipoles ($\vec{r}_{jk}$ is the distance vector of the two interacting magnetic moments). Its Hamilton operator is:[87]

$$\begin{aligned}\hat{H}_D &= \frac{\mu_0}{4\pi}\hbar \sum_{j<k} \gamma_j \gamma_k \frac{3(\vec{I}_j \vec{r}_{jk}/r_{jk})(\vec{I}_k \vec{r}_{jk}/r_{jk}) - \vec{I}_j \vec{I}_k}{r_{jk}^3} \\ &= \sum_{j<k} \vec{I}_j \mathbf{D}_{jk} \vec{I}_j\end{aligned} \tag{19}$$

Here the dipolar interaction tensors $\mathbf{D}_{jk}$ are introduced as a short hand notation of the geometry dependent expression inside the double sum. The secular part of the dipolar Hamiltonian is:

$$\hat{H}_D = \begin{cases} D_{12} 2\vec{I}_{1z}\vec{I}_{2z} & \text{heteronuclear} \\ D_{12}(3\vec{I}_{1z}\vec{I}_{2z} - \vec{I}_1\vec{I}_2) & \text{homonuclear} \end{cases} \tag{20}$$

3.1.5. The Chemical Shift

The next contribution to the local interactions is the chemical shift interaction, which is a result of the interaction of the $\vec{B}_0$-field with the electron cloud surrounding the nucleus.[87] In a semi classical description two different effects are observed: On one hand the external $\vec{B}_0$-field causes a partial orientation, i.e. a polarization, of the orbital magnetic moments of the electron (paramagnetic contribution). On the other hand the external $\vec{B}_0$-field induces ring currents in the electron cloud, which produce, according to the Lenz rule, a field opposite to the $\vec{B}_0$-field (diamagnetic contribution). Employing the chemical shift tensor $\boldsymbol{\sigma}$ the chemical shift Hamiltonian is

$$\hat{H}_{\mathrm{CS}} = \gamma \hat{\vec{I}} \boldsymbol{\sigma} \vec{B}_0. \tag{21}$$

The secular part of the chemical shift Hamiltonian is:

$$\hat{H}_{\mathrm{CS}} = \gamma \sigma_{zz} B_0 \hat{I}_z. \tag{22}$$

3.1.6. The Quadrupolar Interaction

Nuclei with $I > 1/2$ (for example deuterons) exhibit the nuclear quadrupolar interaction as an additional interaction. The quadrupolar interaction describes the coupling of an electric nuclear quadrupolar moment, i.e. a non-spherical charge distribution inside the nucleus, to an electric field gradient. The quadrupolar interaction is described via the so called quadrupolar tensor **Q**. The quadrupolar tensor of NMR is proportional to the electric field gradient tensor **V**. Due to the fact that the electric field and thus the field gradients are mainly determined by bond directions and charge distributions of electrons, the quadrupolar tensor is a very sensitive tool for structural and dynamical studies. The Hamiltonian of the quadrupolar interaction is:

$$\begin{aligned} \hat{H}_{\mathrm{Q}} &= \hat{\vec{I}} \mathbf{Q} \hat{\vec{I}} \\ &= \frac{eQ}{2I(2I-1)\hbar} \hat{\vec{I}} \mathbf{V} \hat{\vec{I}} \end{aligned} \tag{23}$$

In this relation **V** denotes the electric field gradient tensor, i.e. the partial derivatives of an inhomogeneous electric field:

$$\mathbf{V}_{kl} = \frac{\partial E_k}{\partial x_l} = \frac{\partial^2 \phi}{\partial x_k \partial x_l} k, l = x, y, z \tag{24}$$

The secular part of the quadrupolar Hamiltonian is:

$$\hat{H}_{\mathrm{Q}} = \frac{eQ}{2I(2I-1)\hbar} V_{zz} \left(3\hat{I}_z^2 - \hat{\vec{I}}^2\right) \tag{25}$$

3.1.7. The J Coupling

The next interaction is the so called indirect or spin–spin coupling, which is a collection of several interactions which all have the same structure. In particular there is the interaction of the two nuclear spins via spin paired electrons and the exchange interaction of two spin 1/2 nuclei. The J-coupling is also described by a tensor, but in contrast to the dipolar interaction this tensor is not traceless, resulting in a non-vanishing coupling also in isotropic media.

$$\hat{H}_j = \hat{\vec{I}}_1 \mathbf{J}_{12} \hat{\vec{I}}_2 \tag{26}$$

The secular part of the J-coupling Hamiltonian is:

$$\hat{H}_J = \begin{cases} J_{12} \hat{I}_{1z} \hat{I}_{2z} & \text{heteronuclear} \\ J_{12} \hat{\vec{I}}_1 \hat{\vec{I}}_2 & \text{homonuclear} \end{cases} \tag{27}$$

3.1.8. Exchange Interactions of a Spin

The quantum mechanical exchange interaction is the spin Hamiltonian associated with the tunneling of the spins. A general expression for the exchange interaction, valid for all spins, can be written with the help of a permutation operator $\hat{P}\left(\hat{\vec{I}}_1, \hat{\vec{I}}_2\right)$, which exchanges the coordinates of the two spins. In the direct product base $|\mu, v\rangle = |\mu\rangle \otimes |v\rangle$, where $\otimes$ denotes the tensor or direct product of two vector spaces (see for example Refs. 84,89), the matrix elements of the permutation operator are given as:

$$\hat{P}\left(\hat{\vec{I}}_1, \hat{\vec{I}}_2\right) |\mu, v\rangle = |v, \mu\rangle \tag{28}$$

Alternatively if symmetry adapted base functions $|\lambda\rangle$ are employed, the permutation operator is diagonal with diagonal elements $+1$ if the state has even and -1 if the state has odd symmetry.

$$\hat{P}\left(\hat{\vec{I}}_1, \hat{\vec{I}}_2\right) |\lambda\rangle = \pm |\lambda\rangle \tag{29}$$

The exchange Hamiltonian is given as

$$\hat{H}_{\mathrm{x}} = X_{12} \hat{P}\left(\hat{\vec{I}}_1, \hat{\vec{I}}_2\right), \tag{30}$$

where X_{12} is the exchange frequency, which is also called tunnel frequency ν_t or tunnel splitting. Since the permutation Hamiltonian commutes with the Zeeman–Hamiltonian, the secular part of the exchange interaction is identical to (30).

For analytical calculations or larger spin systems, it is advantageous to have a base-independent definition of the permutation operator in terms of spin operators.

Exchange Interactions of Spin $I = 1/2$: For a spin $I = 1/2$ the quantum mechanical exchange interaction was already given by Dirac in the form

$$\hat{H}_X = X\frac{1}{2}\left(1 + 4\hat{\vec{I}}_1, \hat{\vec{I}}_2\right) \tag{31}$$

where the operator in parentheses is a permutation operator, which exchanges the coordinates of the two spins. From the NMR point of view, the eigenfunctions of this Hamiltonian are identical to the eigenfunctions of the normal homonuclear spin–spin interaction and the energy eigenvalues are shifted by a constant offset of $X/2$, since

$$\begin{aligned}\hat{H}_X &= \frac{X}{2} + 2X\hat{\vec{I}}_1, \hat{\vec{I}}_2 \\ &= \frac{X}{2} + J_X\hat{\vec{I}}_1, \hat{\vec{I}}_2\end{aligned} \tag{32}$$

Thus for spin $I = 1/2$ nuclei, the quantum mechanical exchange interaction is formally equivalent to an indirect spin–spin interaction. Accordingly the exchange of spin-1/2 particle is usually treated like a J-coupling (quantum exchange coupling), employing the more simple Hamiltonian

$$\hat{H}'_X = J_X\hat{\vec{I}}_1, \hat{\vec{I}}_2 \tag{33}$$

Exchange Interactions of Spin $I = 1$: In the case of a spin 1 particle the exchange interaction is no longer given by the simple Dirac exchange operator. To achieve a base independent representation we define the following set of normalized single spin operators:

$$\begin{aligned}
B_1 &= \tfrac{1}{\sqrt{2}}S_x & B_2 &= \tfrac{1}{\sqrt{2}}S_y \\
B_3 &= \tfrac{1}{\sqrt{2}}S_z & B_4 &= \tfrac{1}{\sqrt{2}}E \\
B_5 &= \tfrac{1}{\sqrt{2}}\sqrt{6}\left(S_z^2 - \tfrac{2}{3}\right) & B_6 &= \tfrac{1}{\sqrt{2}}\left(S_y^2 - S_x^2\right) \\
B_7 &= \tfrac{1}{\sqrt{2}}\left(S_xS_y + S_yS_x\right) & B_8 &= \tfrac{1}{\sqrt{2}}\left(S_xS_z + S_zS_x\right) \\
B_9 &= \tfrac{1}{\sqrt{2}}\left(S_yS_z + S_zS_y\right)
\end{aligned} \tag{34}$$

Employing these base operators the permutation operator of a homo nuclear spin 1 pair is given by

$$\hat{P}\left(\hat{\vec{I}}_1, \hat{\vec{I}}_2\right) = \sum_k B_k \otimes B_k, \tag{35}$$

which can be shown by inspection.

3.2. Spin Dynamics in Hilbert Space

3.2.1. Wave Functions

Finally some facts about the dynamics of a wave function in Hilbert space, which are used several times in this review for analytic and numerical calculations, should be mentioned. Starting point is the time dependent Schrödinger equation of a single particle, which describes the changes of the particle wave function $|\Psi(t)\rangle$ under the influence of a time dependent Hamiltonian $\hat{H}(t)$:

$$\frac{d}{dt}|\Psi(t)\rangle = -i\hat{H}(t)|\Psi(t)\rangle \tag{36}$$

Two different cases can be distinguished: (i) $\hat{H}$ does not depend explicitly on time: Examples of this situation are all static NMR experiments; (ii) $\hat{H}(t)$ depends explicitly on time. Examples of this situation are all MAS experiments and multi-pulse experiments. In the first situation the Schrödinger equation can be solved by the following unitary propagator:

$$\hat{U}(t, t_0) = \exp(-i\hat{H}(t - t_0)) \tag{37}$$

and the time dependent wave function is given as:

$$|\Psi(t)\rangle = \hat{U}(t, t_0)|\Psi(t_0)\rangle \tag{38}$$

The second situation is more difficult. Two different cases have to be analyzed:

(1) The Hamiltonian is self commuting, i.e.: $[\hat{H}(t_1), \hat{H}(t_2)] = 0$ for all times t_1, t_2.
(2) The Hamiltonian is not self commuting, i.e. $[\hat{H}(t_1), \hat{H}(t_2)] \neq 0$ at least for some times t_1, t_2.

In the first case the kinetic equation can be solved with the help of the following unitary propagator:

$$\hat{U}(t, t_0) = \exp\left(-i\int_{t_0}^{t} \hat{H}(\tau)d\tau\right) \tag{39}$$

The second case needs a more elaborate treatment: The basic idea is to divide the time dependence of the Hamiltonian into a set of finite (or in the limit infinitely narrow) intervals $t_0, t_1, t_2, t_3, \ldots t_n$, such that the Hamiltonians are self commuting in these intervals. Then for each interval a propagator can be calculated and applied to the wave function, according to the previous case. Alternatively it is possible to calculate the total propagator as the time ordered product of the individual propagators,

$$\hat{U}(t_n, t_0) = \hat{U}(t_n, t_{n-1})\hat{U}(t_{n-1}, t_{n-2}) \ldots \hat{U}(t_2, t_1)\hat{U}(t_1, t_0) \tag{40}$$

which can be written in a short hand style with the aid of the Dyson time ordering operator $\hat{T}$:

$$\hat{U}(t, t_0) = \hat{T} \exp\left(-i \int_{t_0}^{t} \hat{H}(\tau) d\tau\right) \tag{41}$$

3.2.2. Density Operator

In most NMR experiments systems of huge numbers of individual spins are under investigation and only statistically averaged information about a system is available. A tool for the description of the dynamics of these systems is the density operator $\hat{\rho}$, also called density matrix or statistical operator, which contains all information extractable from the system. Using $\hat{\rho}$ the expectation value of a physical observable $\langle \hat{A} \rangle$ is given as:

$$\langle \hat{A} \rangle = Tr[\hat{A} \cdot \hat{\rho}] \tag{42}$$

The equation of motion of $\hat{\rho}$ under the influence of the Hamiltonian $\hat{H}$ is:

$$\frac{d}{dt}\hat{\rho} = -i[\hat{H}, \hat{\rho}] \tag{43}$$

This equation can be solved by the same propagators $\hat{U}(t, t_0)$ (Eq. (39) or Eq. (41)) as the Schrödinger equation of the wave function (Eq. (36)):

$$\hat{\rho}(t) = \hat{U}(t, t_0) \cdot \hat{\rho}(t_0) \cdot \hat{U}^{-1}(t, t_0) \tag{44}$$

3.3. Orientation Dependence of Solid State NMR Interactions

Most NMR interactions possess an orientation dependence and are described with interaction tensors **T**, i.e. real symmetric 3×3 matrices.

$$\mathbf{T} = \begin{pmatrix} T_{11} & T_{12} & T_{13} \\ T_{21} & T_{22} & T_{23} \\ T_{31} & T_{32} & T_{33} \end{pmatrix} \tag{45}$$

In high field approximation, if the $\vec{B}_0$-field points into the z-direction, only the T_{zz}-component of these tensors contributes to the spectrum:

$$T_{zz} = \vec{e}_z \mathbf{T} \vec{e}_z \tag{46}$$

There is a close relationship between the orientation of these tensors and molecular structures. This implies that different orientations of, for example, a molecule with respect to the $\vec{B}_0$-field, correspond in general to different values of T_{zz}. For many calculations it is convenient to keep the orientation of the tensor fixed and vary the direction of the external field. Expressing the magnetic field in polar coordinates employing polar angles α and β, the unity vector $\vec{b}$ in the direction of the $\vec{B}_0$-field is

$$\vec{b} = \frac{\vec{B}_0}{B_0} = \begin{pmatrix} \cos\alpha \sin\beta \\ \sin\alpha \sin\beta \\ \cos\beta \end{pmatrix}, \tag{47}$$

which results in the following expression for the secular component of the tensor:

$$T_{zz}(\alpha, \beta) = \vec{b} \mathbf{T} \vec{b} \tag{48}$$

If only a single interaction tensor is present, it is always possible to choose the principle axis system (PAS) of **T** as the coordinate system, resulting in the following expression:

$$T_{zz}(\alpha, \beta) = T_{11} \cos^2\alpha \sin^2\beta + T_{22} \sin^2\alpha \sin^2\beta + T_{33} \cos^2\beta \tag{49}$$

It is convenient to express this equation in a bit different fashion, which is more adapted to the intrinsic symmetry of the tensor, by introducing as new variables the trace of the tensor T_{iso} as its isotropic (spherical symmetric) component, the anisotropy parameter δ, which is a measure of the deviation from spherical symmetry and the asymmetry parameter η, which describes the relative deviation from axial symmetry:

$$\begin{aligned} T_{\text{iso}} &= \frac{1}{3}(T_{11}+T_{22}+T_{33}) \\ \delta &= T_{33}T_{\text{iso}} \\ \eta &= \frac{T_{22}-T_{11}}{T_{33}-T_{\text{iso}}} \end{aligned} \tag{50}$$

Employing these variables Eq. (49) simplifies to:

$$T_{zz}(\alpha,\beta) = T_{\text{iso}} + \frac{1}{2}\delta(3\cos^2\beta - 1 - \eta\sin^2\beta\cos^2\alpha) \tag{51}$$

If single crystals of the sample material are available, the orientation dependence of the NMR transition frequencies can be exploited for determining both principle axes and values of the interaction tensor by recording sets of NMR spectra by rotating the external field in different crystal planes.

Since in this situation a geometric reference frame is already spanned by the rotation axis and the direction of the $\vec{B}_0$-field, there is no more rotational freedom around the $\vec{B}_0$-field and consequently a generalized set of polar angles is necessary for characterizing the mutual orientation of external field, rotation axis and sample, the so-called Euler angles (α, β, γ). With the aid of these three angles it is possible to fully determine the mutual orientation of two different three dimensional coordinate systems. There exist several equivalent definitions of these angles. In the following the definition most common in NMR spectroscopy[94] is used ($R_k(\phi)$: rotation around axis $k = x, y, z$ with angle ϕ):

$$R(\alpha,\beta,\gamma) = R_z(\gamma)R_y(\beta)R_z(\alpha) \tag{52}$$

This rotation can be described as the real 3×3 matrix:

$$R(\alpha,\beta,\gamma) = \begin{pmatrix} \cos\alpha\cos\beta\cos\gamma - \sin\alpha\sin\gamma & \sin\alpha\cos\beta\cos\gamma + \cos\alpha\sin\gamma & -\sin\beta\cos\gamma \\ -\cos\alpha\cos\beta\sin\gamma - \sin\alpha\cos\gamma & -\sin\alpha\cos\beta\sin\gamma + \cos\alpha\cos\gamma & \sin\beta\sin\gamma \\ \cos\alpha\sin\beta & \sin\alpha\sin\beta & \cos\beta \end{pmatrix} \tag{53}$$

The representations of the tensor in the crystal frame and in the PAS frame are related via a rotation ($\alpha_{\text{Pas}}, \beta_{\text{Pas}}, \gamma_{\text{Pas}}$: Euler angles which transfer the PAS frame into the crystal frame):

$$\mathbf{T} = \begin{pmatrix} T_{xx} & T_{xy} & T_{xz} \\ T_{yx} & T_{yy} & T_{yz} \\ T_{zx} & T_{zy} & T_{zz} \end{pmatrix}$$
$$= R(\alpha_{\mathrm{Pas}}, \beta_{\mathrm{Pas}}, \gamma_{\mathrm{Pas}}) \begin{pmatrix} T_{11} & 0 & 0 \\ 0 & T_{22} & 0 \\ 0 & 0 & T_{33} \end{pmatrix} R^{-1}(\alpha_{\mathrm{Pas}}, \beta_{\mathrm{Pas}}, \gamma_{\mathrm{Pas}}) \quad (54)$$

3.3.1. Powder Spectra

Only for few materials single crystals of suitable size for NMR studies are available. Most organic materials, however, exist only as polycrystalline or amorphous powder samples, where a statistical distribution of molecular and thus tensor orientations exists, causing a corresponding distribution of resonance frequencies. The NMR signal is the sum of the contributions of all different orientations present in the sample. If all molecular orientations have equal probability (non-oriented powder sample), this is simply the integral over all possible orientations. The region of the integral depends on the type of problem: in the case of an axial symmetric problem for example, because the direction of the $\vec{B}_0$-field is the only unique direction and therefore the two polar angles describing the direction of the $\vec{B}_0$-field in the tensor frame are sufficient to determine the orientation, it is possible to integrate over the surface of a unit sphere employing the polar angles ϑ and ϕ. In this case the FID is given as:

$$M_+(t) = \frac{1}{4\pi} \int_0^{2\pi} \int_0^{\pi} M_+(t, \phi, \vartheta) \sin\vartheta \, d\vartheta \, d\phi$$
$$= \frac{1}{4\pi} \int_0^{2\pi} \int_0^{\pi} Tr[\hat{I} + \rho(t, \phi, \vartheta)] \sin\vartheta \, d\vartheta \, d\phi. \quad (55)$$

The NMR spectrum is simply the Fourier transform of this time signal. For some special cases (pure chemical shielding, quadrupolar or heteronuclear dipolar interaction) an analytic solution of this double integral in terms of elliptic integrals exists (see Ref. 88). However, in most cases a numerical evaluation of the integral has to be performed.

In the case of no axial symmetry with respect to the $\vec{B}_0$-field, as for example in many MAS experiments, where the coordinate frame is fully determined by the rotation axis and the direction of the $\vec{B}_0$-field, in general a full integration over all three Euler angles has to be performed.

$$M_+(t) = \frac{1}{8\pi^2} \int_0^{2\pi} \int_0^{\pi} \int_0^{2\pi} M_+(t, \alpha, \beta, \gamma) \sin\beta \, d\alpha \, d\beta \, d\gamma \quad (56)$$

3.3.2. ^2H MAS-NMR Distance Measurements of Dipolar Coupled Deuteron Pairs

While solid state NMR techniques are well suited to determine distances of heteronuclear spin pairs like ^{15}N–^{13}C[95] or homonuclear pairs like ^{13}C–^{13}C,[96] they are exceedingly difficult to apply to η^2-bound transition metal complexes, due to presence of hydrogens on the other ligands of many dihydrogen complexes. Therefore only few examples of a successful application of solid state ^1H NMR to determine H–H distances in this class of compounds are known.[45,97,98]

If one is interested in the D–D distance between a homonuclear pair of deuterons the situation becomes even more difficult, since in this situation the strong quadrupolar interaction and the relatively weak homonuclear dipolar coupling, due to the low gyromagnetic ratio of the ^2H nucleus and the comparatively large distances, render it often unfeasible to extract the distance information from the static ^2H NMR spectra. Fortunately the η^2-bonded dideuterium complexes are exceptions of this for the following two reasons: first many of them have short D–D distances with correspondingly strong dipolar couplings and second, the quadrupolar couplings are relatively weak, typically in the range 50–100 kHz, due in part to the high mobility of the hydrons found in these compounds. In this section, a MAS technique is described, which can solve this problem. A detailed analysis of this technique, which is rather elaborate, is found in Facey *et al.*[99] Here, only the results obtained on the labeled Osmium complex $Os(D_2)(Cl)_2(CO)(P^iPr_3)_2$ are presented as an example of this MAS-technique.

Figure 8a displays the slow spinning (4000 Hz) ^2H MAS NMR spectrum of the Os-D_2 complex at 30.7 MHz. A striking feature of the MAS spectrum is the broadening of the base of the individual side bands. The enlargement shows that the line shape of the individual side bands resembles a typical Pake line shape with additional spectral intensity in the center of the side band. On closer inspection of the line shape of these side bands it is evident that there is some variation in the actual width and form of the line shape as a function of the side band order. A detailed numerical and theoretical discussion given in Ref. 99 shows that these Pake like side band patterns are the result of an interference effect between the ^2H-homonuclear dipolar and ^2H-quadrupolar interaction.

For the numerical analysis of the D–D distance, the individual sidebands are collapsed onto a single line and this line is fitted by a numerical simulation. The best fit (Fig. 8b) was obtained for a dipolar coupling of $D = 3.2 \pm 0.2$ kHz, corresponding to a DD-distance of 0.96 ± 0.02 Å and an

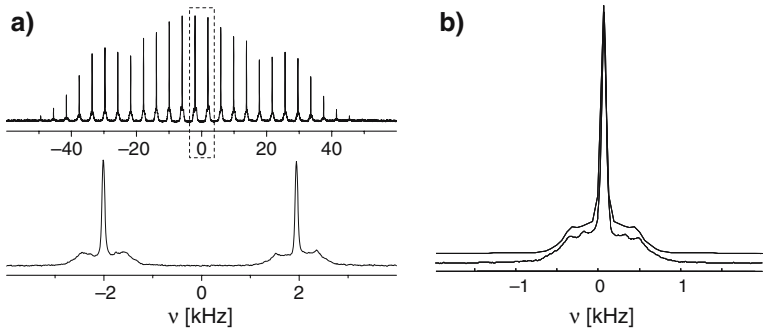

Fig. 8. (a) ^{2}H-MAS-NMR spectrum of O_S-D_2 complex obtained at 4000 Hz spinning speed and enlargement of the central two side bands (dashed rectangle). The spinning side bands clearly exhibit a Pake like shape. (b) Comparison of the collapsed experimental side band spectrum and the fitted average Hamiltonian spectrum ($\nu_{ROT} = 4000$ Hz, $2\beta = 0°$, D = 3.2 kHz).

angle of $2\beta = 0°$ for the mutual orientation of the tensors. The resulting angle shows that the two deuterons are in fast exchange.

It is interesting to compare the D–D distance obtained from the AVH spectrum to the distance obtained from the H–H isotopomer. In solution an H–H distance of between 0.9 and 1.1 Å was estimated from the minimum T_1 of the H_2 complex, with the 1.1 Å value considered to be more likely on the basis of the small ^1J (HD) value of the HD isotopomer.[100,101] Thus the D–D distance is comparable to the H–H distance but slightly shorter. While part of this shortening could be the result of the DD stretching vibration, which, due to the $< r^{-3} >$ averaging of NMR, favors shorter distances it is also an indication of an isotope effect on the distance, possibly due to a shift of the average deuteron positions in the anharmonic potential.

3.4. Chemical Kinetics and Liouville Space

This section summarizes the basic formalism for the description of chemical dynamics and exchange processes in two-site systems. Readers interested in a more extensive coverage of the field are referred to the recent review article by Bain.[102] The description given here is restricted to first order kinetics. The basic idea of this formalism is that the time scale of a chemical reaction or an exchange process is fast compared to the NMR time scale. Under this assumption the chemical reaction leads to a fluctuating time dependence of the spin-Hamiltonian and it is permissible to treat the reaction as an instantaneous exchange between different

molecular configurations, described by different static Hamiltonians, without having to take into account the actual reaction coordinates or pathway.

The description of chemical exchange processes is most easily done in a composite Liouville space, which is the tensorial sum of Liouville spaces corresponding to the individual Hamiltonians, i.e. to a single molecular configuration, which in the following is called a site. For the case of mutual exchange of protons the resulting theory is a generalized version of the original Alexander–Binsch[51,52] theory for the calculation of exchange broadened ^{1}H-liquid state NMR spectra. From the NMR point of view two cases have to be distinguished:

(1) Chemical exchange between sites with different chemical shielding, quadrupolar interactions or heteronuclear dipolar interactions. In this situation all Hamiltonians are diagonal in the same base set and it is possible to simply solve the equation of motion of the various single spin operators $\hat{I}_x$ or $\hat{I}_+$, i.e. in a small subspace of the composite Liouville space, resulting in a relatively small set of coupled linear differential equations.
(2) Chemical exchange in the presence of homonuclear couplings or more general non-diagonal Hamiltonians. In most cases it is impossible to find a single base, which simultaneously renders all Hamiltonians to be diagonal.

As a model, which covers most features of exchange processes, the equations of motion of a single spin, exchanging between two sites with different resonance frequencies (for example different isotropic chemical shielding in a liquid or different chemical shielding anisotropy due to a reorientation jump in a solid) with reaction rates k_{12} and k_{21} respectively, are discussed. The two sites are characterized by their individual site Hamiltonians:

$$\begin{aligned} \hat{H}_1 &= \omega_1 \hat{I}_{1z} \\ \hat{H}_2 &= \omega_2 \hat{I}_{2z} \end{aligned} \tag{57}$$

First two limiting cases can be distinguished: (i) the reaction rates are zero, ($k_{12} = k_{21} = 0$). In this case the resulting spectrum is just the superposition of two lines, observed at resonance frequencies ω_1 and ω_2. (ii) the exchange is much faster than the frequency difference, i.e.: ($|k_{12} - k_{21}| \sim |\omega_1 - \omega_2|$). In this situation the fast exchange leads to a weighted average of the two Hamiltonians ($\bar{\omega}$: weighted average frequency):

$$\begin{aligned}\hat{\bar{H}} &= \frac{k_{12}}{k_{12}+k_{21}}\hat{H}_1 + \frac{k_{12}}{k_{21}+k_{12}}\hat{H}_2 \\ &= \bar{\omega}\hat{I}_z \end{aligned} \tag{58}$$

If neither of these two conditions is fulfilled the equation of motion of the density matrix has to be solved:

$$\begin{aligned}\frac{d}{dt}|\rho_1) &= -\hat{\hat{W}}_1|\rho_1) - k_{12}|\rho_1) + k_{21}|\rho_2) \\ \frac{d}{dt}|\rho_2) &= -\hat{\hat{W}}_1|\rho_1) - k_{21}|\rho_2) + k_{12}|\rho_1) \end{aligned} \tag{59}$$

Here $|\rho_1)$ and $|\rho_2)$ denote the density matrices in the two subspaces of Liouville space and $\hat{\hat{W}}_n = \hat{\hat{L}}_n + \hat{\hat{R}}_n$ (with $n = 1, 2$) is a superoperator which describes the coherent dynamics $\hat{\hat{L}}_n$ and the relaxation $\hat{\hat{R}}_n$ in the two sites. For simplicity it is assumed that the relaxation superoperators $\hat{\hat{R}}_n$ are simply Bloch type operators, i.e. diagonal with two characteristic relaxation times T_1 and T_2. The subspace Liouville operators $\hat{\hat{L}}_n$ can be constructed from the site Hamiltonians:

$$\hat{\hat{L}}_n = \hat{H}_n \otimes \hat{E}_n - \hat{E}_n \otimes \hat{H}_n \tag{60}$$

The exchange superoperator $\hat{\hat{K}}$, which connects the two subspaces of composite Liouville space is given as the direct product of the reaction matrix and the identity operators $\hat{\hat{E}}_n$ in the subspaces:

$$\hat{\hat{K}} = \begin{pmatrix} -k_{12} & k_{21} \\ k_{12} & -k_{21} \end{pmatrix} \otimes \hat{\hat{E}}_n \tag{61}$$

In composite Liouville space the density operator and the Liouville and relaxation superoperators are the direct sums of their counterparts in the subspaces:

$$\begin{aligned} |\rho) &= |\rho_1) \oplus |\rho_2) \\ \hat{\hat{L}} &= \hat{\hat{L}}_1 \oplus \hat{\hat{L}}_2 \\ \hat{\hat{R}} &= \hat{\hat{R}}_1 \oplus \hat{\hat{R}}_2 \\ \hat{\hat{W}} &= \hat{\hat{W}}_1 \oplus \hat{\hat{W}}_2 \end{aligned} \tag{62}$$

The coupled differential equations Eq. (59) become a single equation in composite Liouville space

$$\frac{d}{dt}|\rho) = \left(-\hat{\hat{W}} + \hat{\hat{K}}\right)|\rho) =: -\hat{\hat{M}}|\rho). \tag{63}$$

where for brevity $\hat{\hat{M}}_2$ is introduced as the "dynamical superoperator". If $\hat{\hat{M}}_2$ does not explicitly depend on time, the solution of Eq. (63) is

$$|\rho(t)) = \exp(-\hat{\hat{M}}t)|\rho(0)). \tag{64}$$

If the system is treated at finite temperature, the equilibrium density matrix will be different from zero, and the Liouville–von Neumann equation is obtained as the kinetic equation of the density matrix

$$\frac{d}{dt}|\rho) = -\hat{\hat{M}}\,|\,\rho - \rho_\infty), \tag{65}$$

with the solution

$$|\rho(t)) = \exp(-\hat{\hat{M}}t)|\rho(0) - \rho_\infty) + |\rho_\infty). \tag{66}$$

3.4.1. Incoherent Exchange in the Presence of Diagonal Hamiltonians

If the site-Hamiltonians are diagonal in the Zeeman base, only a small subspace of the Liouville space, which is spanned by the operators $\hat{I}_{1+}$ and $\hat{I}_{2+}$, contributes to the NMR FID or spectrum. Choosing these operators as base operators of this subspace, the FID (the time evolution of the magnetization $M_+(t)$) is

$$M_+(t) = \begin{pmatrix} 1 \\ 1 \end{pmatrix} \exp\left(\begin{pmatrix} -k_{12} - r_1 - i\omega_1 & k_{21} \\ k_{12} & -k_{21} - r_2 - i\omega_2 \end{pmatrix} t \right) \begin{pmatrix} p_1 \\ p_2 \end{pmatrix}, \tag{67}$$

where p_1 and p_2 are the respective initial populations of site 1 and site 2. For a quantitative evaluation, it is most convenient to diagonalize the 2×2 matrix and transform the equation into the eigenbase of the matrix:

$$M_+(t) = \begin{pmatrix} 1 \\ 1 \end{pmatrix} S \cdot \exp \begin{pmatrix} \lambda_1 t & 0 \\ 0 & \lambda_2 t \end{pmatrix} \cdot S^{-1} \cdot \begin{pmatrix} p_1 \\ p_2 \end{pmatrix} \tag{68}$$

Evaluating the scalar products gives the FID:

$$\begin{aligned} M_+(t) &= (S_{11}^{-1} + S_{21}^{-1}) + (S_{11}p_1 + S_{12}p_2)\exp(\lambda_1 t) \\ &\quad + (S_{12}^{-1} + S_{22}^{-1})(S_{21}p_1 + S_{22}p_2)\exp(\lambda_2 t) \\ &= c_1 \exp(\lambda_1 t) + c_2 \exp(\lambda_2 t) \end{aligned} \tag{69}$$

Fourier transforming yields the spectrum, a superposition of two complex Lorentzian lines:

$$M_+(\omega) = c_1 \frac{1}{-\lambda_1 + i\omega} + c_2 \frac{1}{-\lambda_2 + i\omega} \tag{70}$$

It is possible to immediately generalize these results to describe larger exchanging systems, provided that the Hamiltonians of the individual sites have the Zeeman base as a common eigenbase.[89]

3.4.2. Incoherent Exchange in the Presence of Non-Diagonal Hamiltonians

The situation is more elaborate, if homonuclear couplings are present, or more generally, if some or all of the involved Hamiltonians are non-diagonal. In this situation two different cases can be distinguished: If the Hamiltonians have a common eigenbase, i.e., if it is possible to simultaneously diagonalize them, the exchange problem reduces after transformation of the detection operator $(\hat{I}_+|$ and the initial density operator $|\rho_0)$ to the previous case.

If it is not possible to simultaneously diagonalize both Hamiltonians, as for example in the numerical and analytical simulations of *para*-hydrogen induced polarization experiments (^{1}H-PHIP)[50] and ^{2}H exchange and tunnel spectra, a different strategy has to be applied. If the same spin base functions are used for both sites, the problem is describable by the same set of coupled differential equations as Eqs. (63) and (65). However, in general it is no longer possible to achieve a blocking of the dynamic superoperator in sets of 2×2 matrices by choosing for example the $\hat{I}_+$ operators as base operators of Hilbert space. Therefore the evaluation of the density operator occurs in larger subspaces, making it necessary to either evaluate the full matrix exponential or alternatively to search for suitable subspaces, which transform $\hat{\hat{M}}$ into a block diagonal form.

3.4.3. NMR-Line Shape Analysis of Tunneling Systems

This section is devoted to a discussion of the analysis of NMR line shapes and relaxation data for elucidation and interpretation of coherent and incoherent rate constants.

As a starting point of this discussion a very basic question from quantum mechanics, regarding indistinguishable particles has to be shortly addressed: One of the basic postulates of quantum mechanics states that the wave function of identical particles must be symmetric or anti-symmetric. Thus in theory it is not possible to observe the motion of an individual H-atom in an H_2-system. By NMR however it is possible for all practical purposes to follow this motion, owing to the fact that NMR does not observe the nuclear motion of individual hydrons, but changes in the

resonance frequencies of nuclear spin states of a large ensemble of spins (weak measurement). These changes of frequency are interpreted as the result of a physical exchange of the hydrons and not as the result of a spin or magnetization exchange of the hydrons, which would lead to the same spectrum. Thus the following discussion does not violate the basic principles of quantum mechanics.

Starting point of the description of the effect of coherent tunneling on the ^{2}H NMR spectra are the spin Hamiltonians in high field approximation. The relevant contributions are in the first approximation the quadrupolar interaction $\hat{H}_{\mathrm{Q}}$ and the coherent tunnel exchange interaction $\hat{H}_{\mathrm{X}}$:

$$\begin{aligned}\hat{H} &= \hat{H}_{\mathrm{Q}} + \hat{H}_{\mathrm{X}} \\ &= q_1\left(\hat{I}_{1z}^2 - \frac{2}{3}\right) + q_2\left(\hat{I}_{2z}^2 - \frac{2}{3}\right) + X_{12}\hat{P}\left(\hat{\vec{I}}_1, \hat{\vec{I}}_2\right)\end{aligned} \tag{71}$$

In these equations, q_1 and q_2 are the quadrupolar couplings of the spins, X_{12} is the coherent tunnel frequency, $\hat{P}\left(\hat{\vec{I}}_1, \hat{\vec{I}}_2\right)$ is the permutation operator of the two spins in spin space. If the nine Zeeman product functions of the two-spin system are chosen as base functions the matrix representation of the Hamiltonian is

$$\hat{H} = \begin{pmatrix}
X_{12}+\frac{2}{3}Q & 0 & 0 & 0 & 0 & 0 & 0 & 0 & 0 \\
0 & -\frac{1}{3}Q-q & 0 & X_{12} & 0 & 0 & 0 & 0 & 0 \\
0 & 0 & \frac{2}{3}Q & 0 & 0 & 0 & X_{12} & 0 & 0 \\
0 & X_{12} & 0 & -\frac{1}{3}Q+q & 0 & 0 & 0 & 0 & 0 \\
0 & 0 & 0 & 0 & X_{12}-\frac{4}{3}Q & 0 & 0 & 0 & 0 \\
0 & 0 & 0 & 0 & 0 & -\frac{1}{3}Q+q & 0 & X_{12} & 0 \\
0 & 0 & X_{12} & 0 & 0 & 0 & \frac{2}{3}Q & 0 & 0 \\
0 & 0 & 0 & 0 & 0 & X_{12} & 0 & -\frac{1}{3}Q-q & 0 \\
0 & 0 & 0 & 0 & 0 & 0 & 0 & 0 & X_{12}+\frac{2}{3}Q
\end{pmatrix}$$

which can be diagonalized analytically. The eigenvalues and corresponding eigenvectors are shown in the following table

$E_{1,2,3} = X_{12} + \frac{2}{3}Q$	$\|1\rangle = \|++\rangle$ $\|2\rangle = \|--\rangle$ $\|3\rangle = \frac{1}{\sqrt{2}}(\|+-\rangle + \|-+\rangle)$
$E_{4,5} = -\frac{1}{3}Q - \sqrt{X_{12}^2 + q^2}$	$\|4\rangle = \frac{1}{\sqrt{2}}(\cos\phi\|-0\rangle - \sin\phi\|0-\rangle)$ $\|5\rangle = \frac{1}{\sqrt{2}}(-\sin\phi\|0+\rangle + \cos\phi\|+0\rangle)$
$E_{6,7} = -\frac{1}{3}Q + \sqrt{X_{12}^2 + q^2}$	$\|6\rangle = \frac{1}{\sqrt{2}}(\cos\phi\|0-\rangle + \sin\phi\|-0\rangle)$ $\|7\rangle = \frac{1}{\sqrt{2}}(\sin\phi\|+0\rangle + \cos\phi\|0+\rangle)$
$E_8 = X_{12} - \frac{4}{3}Q$	$\|8\rangle = \|00\rangle$
$E_9 = -X_{12} + \frac{2}{3}Q$	$\|9\rangle = \frac{1}{\sqrt{2}}(-\|+-\rangle + \|-+\rangle)$

(72)

where the angle ϕ is defined via $\tan\phi = \frac{q+\sqrt{q^2+X_{12}^2}}{X_{12}}$.

In contrast to the coherent exchange interaction the quadrupolar interaction depends on the relative orientation of the magnetic field to the quadrupolar tensor. Since both deuterons can be assumed to be chemically equivalent, their quadrupolar tensors are related by a geometrical transformation. If we assume C_{2v} symmetry of the M-D_2 group by neglecting possible crystal effects, one of the three principal axes of the quadrupolar tensor will be perpendicular to the M-D_2 plane, and the axis bisecting the bond angle (2α) will be a twofold symmetry axis (C_2). A coordinate system (Fig. 9) is chosen in such a way that the z-axis bisects the bond angle and that the y-axis is perpendicular to the bond plane. The two quadrupolar tensors are related by a rotation $R(\beta)$ with angles $\pm\beta$ around the y-axis of the coordinate system. The angle β depends on the strength of the electric field gradients caused by the metal and by the other deuterons. In particular in the case of a dihydride, β will be half the bond angle (i.e. $\beta = \alpha$). For molecular dihydrogen with a very weak interaction with the metal or dihydrogen complexes, where the M–D bonding is negligible compared to the D–D bonding, the two quadrupolar tensors will have their z-axis in the direction of the D–D axis, i.e. : $\beta = \pi/2$. For simplicity we will call these complexes pure dihydrogen complexes.

The quadrupolar tensors in the molecular coordinate system ($\mathbf{Q}_1$ and $\mathbf{Q}_1$) are related to the quadrupolar tensor in its principal axis sys-

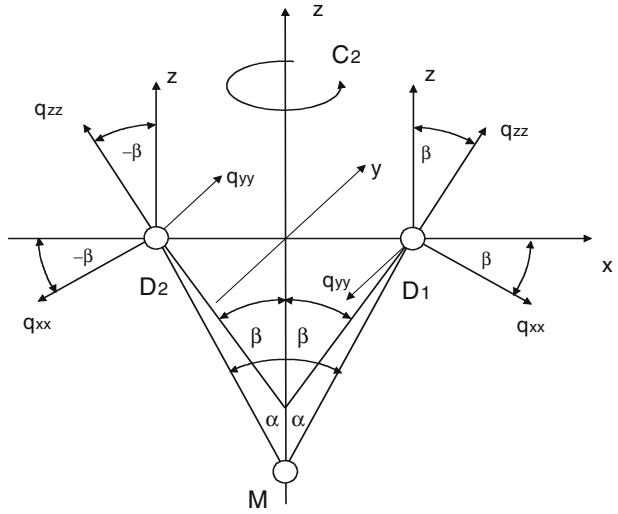

Fig. 9. M-H_2 coordinate system used for the description of the relative spatial orientation of the two quadrupolar tensors of deuterons D_1 and D_2. C_{2v} symmetry is assumed for the deuterons and therefore one of the principal axis (q_{yy}) is parallel to y. The quadrupolar tensor of deuteron D_2 is obtained by a 180° rotation around the z-axis of the coordinate system. For describing the relative orientations of the tensors it is more convenient to use the angle between the z-axis and the q_{zz}-component. Note that in general the bond angle 2α will not coincide with the jumb angle 2β, i.e. $2\alpha \neq \beta$.

tem ($\mathbf{Q}_{\mathrm{PAS}}$) via the following rotations

$$\begin{aligned} \mathbf{Q}_1 &= R(\beta)\tilde{\mathbf{Q}}_{\mathrm{PAS}}R^{-1}(\beta) \\ \mathbf{Q}_2 &= R^{-1}(\beta)\tilde{\mathbf{Q}}_{\mathrm{PAS}}R(\beta) \end{aligned} \tag{73}$$

The rotation matrix $R(\beta)$ is

$$R(\beta) = \begin{pmatrix} \cos\beta & 0 & -\sin\beta \\ 0 & 1 & 0 \\ \sin\beta & 0 & \cos\beta \end{pmatrix} \tag{74}$$

and the quadrupolar tensors become (q_{xx}, q_{yy}, q_{zz}: principal values of the quadrupolar interaction):

$$\mathbf{Q}_{1,2} = \begin{pmatrix} q_{xx}\cos^2\beta + q_{zz}\sin^2\beta & 0 & \pm(q_{xx}-q_{zz})\cos\beta\sin\beta \\ 0 & q_{yy} & 0 \\ \pm(q_{xx}-q_{zz})\cos\beta\sin\beta & 0 & q_{xx}\sin^2\beta + q_{zz}\cos^2\beta \end{pmatrix} \tag{75}$$

The quadrupolar frequencies are calculated from $\mathbf{Q}_{1,2}$ employing Eq. (48).

In the absence of incoherent exchange processes, the whole dynamics of the system can be described directly in Hilbert space and the spectra can be calculated directly from $\hat{H}$. However, as soon as incoherent exchange mechanisms are present, this approach is no longer valid. A method for tackling this type of problems is the generalized Alexander–Binsch formalism.

3.4.4. Generalized Alexander–Binsch Theory and Incoherent Dynamics

In this section a formulation of simultaneous coherent (tunneling) and incoherent exchange processes of dihydrogen and dideuterium is given, using a density matrix formalism which is a generalized version of the original Alexander–Binsch theory for the calculation of exchange broadened NMR spectra of mutually exchanging protons. The idea behind this theory is to treat the incoherent exchange caused by the fluctuating time dependence of the parameters in the Hamiltonian as above and include an additional coherent exchange spin Hamiltonian which describes the tunneling.

The incoherent exchange occurs between several molecular configurations (denoted by capital letters A,B,...) with an exchange rate which is determined by the rate of the fluctuation. In the following, for brevity these molecular configurations are called states.

The various dihydrogen states (n) are characterized by their basic spin Hamiltonians $\hat{H}_n$, respectively by their state Liouville superoperators $\hat{\hat{L}}_n$, which are combined to the composite Liouville space. In this composite Liouville space the solution of the Liouville–von Neumann equation Eq. (65) has to be computed.

3.4.5. The Self Exchange Operator

In the following a derivation of the self exchange operator, i.e. the operator of the coherent mutual exchange of two identical particles and an analysis of its properties are given.

In the case of a mutual exchange of two equal nuclei, for example two protons or two deuterons as in our case, permutation symmetries in the Hamiltonian will lead to a projection of the whole Liouville space onto a subspace, as shown below. In this case the mutual exchange of the two nuclei corresponds to a permutation of the two nuclei which exchanges their individual quadrupolar couplings in Eq. (71).

In this case, because of the symmetry of the problem, it follows that: $k_{12} = k_{21} = k$. The Hamiltonian of the system consists of three parts. The

individual Hamiltonians of the spins $\hat{\vec{I}}_1$ and $\hat{\vec{I}}_2$, which are most easily described by assigning them to molecular sites $m := 1, 2$ i.e.: $\hat{H}_m\left(\hat{\vec{I}}_1\right)$ is the Hamiltonian of spin n in site m; and a Hamiltonian $\hat{H}_{1,2}\left(\hat{\vec{I}}_1, \hat{\vec{I}}_2\right)$ describing the coupling between the two spins. Due to the permutation symmetry of the two nuclei the latter is necessarily invariant under the permutation of the two nuclei, i.e. commutes with the permutation operator $\hat{P}\left(\hat{\vec{I}}_1, \hat{\vec{I}}_2\right)$.

The incoherent process is then a permutation of the individual Hamiltonians with rate k, i.e.:

$$\left\{\begin{array}{l}\hat{H}_1\left(\hat{\vec{I}}_1\right)\\ \hat{H}_2\left(\hat{\vec{I}}_2\right)\end{array}\right\} \overset{k}{\longleftrightarrow} \left\{\begin{array}{l}\hat{H}_1\left(\hat{\vec{I}}_1\right)\\ \hat{H}_2\left(\hat{\vec{I}}_2\right)\end{array}\right\}, \tag{76}$$

which can be regarded as a fluctuation between $\hat{H}_\mathrm{a}$ and $\hat{H}_\mathrm{b}$ with the rate k:

$$\begin{aligned}\hat{H}_a &= \hat{H}_1\left(\hat{\vec{I}}_1\right) + \hat{H}_2\left(\hat{\vec{I}}_2\right) + \hat{H}_{12}\left(\hat{\vec{I}}_1, \hat{\vec{I}}_2\right)\\ \hat{H}_b &= \hat{H}_2\left(\hat{\vec{I}}_1\right) + \hat{H}_1\left(\hat{\vec{I}}_2\right) + \hat{H}_{12}\left(\hat{\vec{I}}_1, \hat{\vec{I}}_2\right)\end{aligned} \tag{77}$$

The equations of motion for the density operator Eq. (59) reduce to:

$$\begin{aligned}\frac{d}{dt}|\rho_\mathrm{A}\rangle &= -\hat{\hat{W}}_\mathrm{A}|\rho_\mathrm{A}\rangle - k|\rho_\mathrm{A} - \rho_\mathrm{B}\rangle\\ \frac{d}{dt}|\rho_\mathrm{B}\rangle &= -\hat{\hat{W}}_\mathrm{B}|\rho_\mathrm{B}\rangle - k|\rho_\mathrm{B} - \rho_\mathrm{A}\rangle\end{aligned} \tag{78}$$

In Liouville space, the permutation of the two nuclei is described by a permutation superoperator $\hat{\hat{P}}_{12}$, which is constructed from the permutation operator in Hilbert space $\hat{P}\left(\hat{\vec{I}}_1, \hat{\vec{I}}_2\right)$

$$\hat{\hat{P}} = \hat{P}\left(\hat{\vec{I}}_1, \hat{\vec{I}}_2\right) \otimes \left(\hat{\vec{I}}_1, \hat{\vec{I}}_2\right)^* \tag{79}$$

where $\hat{P}\left(\hat{\vec{I}}_1, \hat{\vec{I}}_2\right)^*$ denotes the complex conjugate of operator $\hat{P}\left(\hat{\vec{I}}_1, \hat{\vec{I}}_2\right)$. Since $\hat{\hat{P}}_2$ is a permutation superoperator, applying it twice gives the identity $\hat{\hat{I}}_\mathrm{d}$.

$$\hat{\hat{P}}_{12}\hat{\hat{P}}_{12} = \hat{\hat{I}}_\mathrm{d} \text{ i.e. } \hat{\hat{P}}_{12} = \hat{\hat{P}}_{12}^{-1} \tag{80}$$

Employing $\hat{\hat{P}}_{12}$, the permutation symmetry of the nuclei is expressed as:

$$\hat{\hat{W}}_A = \hat{\hat{P}}_{12}\hat{\hat{W}}_B - \hat{\hat{P}}_{12}^{-1} \tag{81}$$

In a matrix representation the equation of motion for the density matrix in composite Liouville space has the following form

$$\frac{d}{dt}\begin{pmatrix}\rho_a\\ \rho_b\end{pmatrix} = \begin{pmatrix} -\hat{\hat{W}}_A - k\hat{\hat{I}}_d & k\hat{\hat{I}}_d \\ k\hat{\hat{I}}_d & -\hat{\hat{W}}_B - k\hat{\hat{I}}_d \end{pmatrix}\begin{pmatrix}\rho_a\\ \rho_b\end{pmatrix}, \tag{82}$$

which can be transformed by the superoperator

$$\begin{pmatrix} \hat{\hat{I}}_d & 0 \\ 0 & \hat{\hat{P}}_{12} \end{pmatrix} \tag{83}$$

into

$$\frac{d}{dt}\begin{pmatrix}\rho_a\\ \hat{\hat{P}}_{12}\rho_b\end{pmatrix} = \begin{pmatrix} -\hat{\hat{W}}_A - k\hat{\hat{I}}_d & k\hat{\hat{P}}_{12} \\ k\hat{\hat{P}}_{12} & \hat{\hat{W}}_A - k\hat{\hat{I}}_d \end{pmatrix}\begin{pmatrix}\rho_a\\ \hat{\hat{P}}_{12}\rho_b\end{pmatrix}. \tag{84}$$

This matrix differential equation can be block diagonalized with the help of the symmetric ρ_g and asymmetric ρ_u linear combinations of ρ_A and $\hat{\hat{P}}_{12}\rho_B$. The decoupled differential equations are

$$\begin{aligned}\frac{d}{dt}\begin{pmatrix}\rho_g\\ \rho_u\end{pmatrix} &= \frac{d}{dt}\begin{pmatrix}\rho_a + \hat{\hat{P}}_{12}\rho_b\\ \rho_a - \hat{\hat{P}}_{12}\rho_b\end{pmatrix} \\ &= \begin{pmatrix} -\hat{\hat{W}}_A - k(\hat{\hat{I}}_d - \hat{\hat{P}}_{12}) & 0 \\ 0 & \hat{\hat{W}}_A - k(\hat{\hat{I}}_d - \hat{\hat{P}}_{12}) \end{pmatrix}\frac{d}{dt}\begin{pmatrix}\rho_a + \hat{\hat{P}}_{12}\rho_b\\ \rho_a - \hat{\hat{P}}_{12}\rho_b\end{pmatrix}.\end{aligned} \tag{85}$$

These transformations are projections of the complete Liouville space into the symmetric L_g and anti symmetric L_u subspace. Because of the symmetry of the states, the initial condition in normal NMR experiments will be $\rho_A(0) = \hat{\hat{P}}_{12}\rho_B(0)$ and thus the anti symmetric density matrix is zero initially ($\rho_u(0) = 0$) and hence for all times and only the symmetric subspace L_g has to be considered in the time evolution of the density matrix, which gives the following equation for ρ_g:

$$\begin{aligned}\frac{d}{dt}|\rho_g) &= -\hat{\hat{W}}_A - k(\hat{\hat{I}}_d - \hat{\hat{P}}_{12})|\rho_g) \\ &= -(\hat{\hat{W}}_A + \hat{\hat{K}}|\rho_g)\end{aligned} \tag{86}$$

where the self-exchange superoperator $\hat{\hat{K}}$ is introduced:

$$\hat{\hat{K}} = -k(\hat{\hat{I}}_{\mathrm{d}} - \hat{\hat{P}}_{12}) \tag{87}$$

This formal derivation of the self-exchange can be interpreted using a physical picture. In the symmetric linear combination of the individual density matrices, the two spins have lost their individuality. However, the individual Hamiltonians are still distinct and correspond usually to different molecular or, more generally, different spatial sites, which are characterized by their NMR parameters. Thus, the labeling of the spins is done via these sites (1, 2), and is sometimes called site labeling.

3.4.6. Physical Properties of the Self Exchange Operator

To understand the physical properties of the self exchange operator, it is most useful to use the representation of the permutation operator $\hat{P}\left(\hat{\vec{I}}_1, \hat{\vec{I}}_2\right)$ in a symmetry adapted base, where it is diagonal with diagonal elements ± 1 (see Eq. (29)). If μ is an index, which denotes the symmetry of the eigenfunction the matrix representation is (δ_{jk}: Kronecker symbol):

$$\hat{P}\left(\hat{\vec{I}}_1, \hat{\vec{I}}_2\right)_{jk} = (-1)^{\mu}\delta_{jk} \text{ where } \begin{cases} \mu = 0: & \text{even} \\ \mu = 1: & \text{odd} \end{cases} \tag{88}$$

A simple calculation (see Ref. 8 for details) shows that the permutation superoperator in Liouville space $\hat{\hat{P}}_{12}$ is diagonal in this base, with matrix elements which are either $+1$, if states of the same symmetry $\mu = \lambda$ are connected, or -1, if states of different symmetry $\mu \neq \lambda$ are connected:

$$(\hat{\hat{P}}_{12})_{ij,kl} = \delta_{ij} \cdot \delta_{kl} \cdot \begin{cases} +1 & \mu = \lambda \\ -1 & \mu \neq \lambda \end{cases} \tag{89}$$

For simplicity double indices from the Hilbert space base are used as indices for the Liouville space. In this base the self-exchange superoperator $\hat{\hat{K}}$ is also diagonal with matrix elements 0, if states of the same symmetry are connected and matrix elements $-2k$, if states of different symmetry are connected:

$$\hat{\hat{K}}_{ij,kl} = -k\left(\delta_{ij} \cdot \delta_{kl} \cdot \begin{cases} 0 & \mu = \lambda \\ 2 & \mu \neq \lambda \end{cases}\right). \tag{90}$$

This result can be interpreted using a simple physical picture: In the symmetry adapted base, the self-exchange operator acts as a relaxation operator for coherences created between the states of different symmetry, which relax with the rate $-2k$. It is important to note that this result is not restricted to NMR but is also valid for INS for example, where $\hat{\hat{K}}$ creates broadening of the energy loss and energy gain transitions.

3.4.7. *Exchange Processes Monitored via ^{2}H-Spin–Lattice Relaxation*

Besides affecting the shape of the ^{2}H NMR spectra, coherent and incoherent exchange effects can also influence the ^{2}H-spin–lattice relaxation rates. Assuming that mainly the incoherent exchange and classical over the barrier motion will contribute to the spin–lattice relaxation rate, in particular at higher temperatures, there is a direct relation between the characteristic time constant τ_c in the spectral density functions in the relaxation model and the incoherent exchange rates k:

$$\tau_c(T) = \frac{1}{2k_{12}} \tag{91}$$

The actual spin–lattice relaxation rate depends on the motional model of the exchange process.[103] In the general case, where the motional model is not known exactly, an effective coupling rate constant K^{EFG} can be used.[87]

$$\frac{1}{T_1} = K^{EFG} J(\tau) \tag{92}$$

Several special types of motions are discussed in the literature: (a) isotropic rotational diffusion[104] (Eq. (93)), (b) jump motions of the deuterons employing the model of[105,106] (note: Eq. (94) is calculated from the single crystal value given in reference[106] by integrating the relaxation over all possible crystal orientations); (c) axial symmetric rotational diffusion[104] (Eq. (95)). If $J(\tau)$ describes the spectral density function of the fluctuations, the corresponding relaxation functions are

$$\frac{1}{T_1} = 0.3\pi^2 q_{cc}^2 J(\tau), \tag{93}$$

$$\frac{1}{T_1} = \frac{9}{160} \sin^2 \beta q_{cc}^2 J(\tau), \tag{94}$$

$$\frac{1}{T_1} = 0.3\pi^2 q_{cc}^2 \left(\frac{1}{4}(\cos^2 \beta - 1) J(\tau_0) + 3 \sin^2 \beta \cos^2 \beta J(\tau_1) + \frac{3}{4} \sin^4 \beta J(\tau_2) \right). \tag{95}$$

τ or (τ_0, τ_1, τ_2) are correlation times of isotropic and anisotropic motions, respectively. β is the angle between rotation axis and tensor axis (and relates to the angle between the two tensor axes). $J(\tau)$ is the usual spectral density function of the fluctuations

$$J(\tau) = \left(\frac{\tau}{1 + \omega^2 \tau^2} + \frac{4\tau}{1 + 4\omega^2 \tau^2} \right). \tag{96}$$

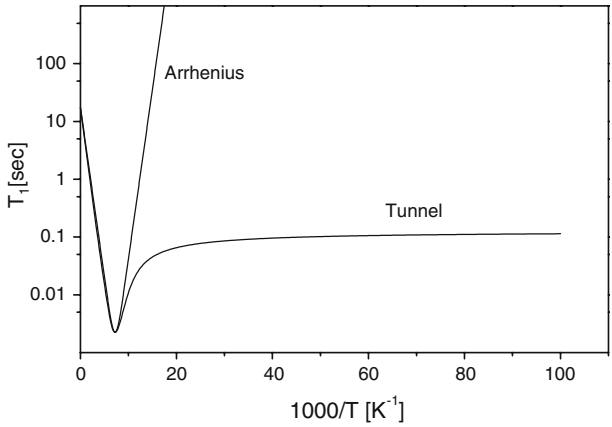

Fig. 10. T_1 temperature dependence: Arrhenius and tunnel process (Bell model). The plateau in the tunnel process is the result from the plateau in the incoherent tunnel rate calculated in the Bell model (see Fig. 6d).

The overall differences in the shapes of the relaxation curves, calculated with these models, are relatively small over large temperature ranges. For an Arrhenius dependence of τ on the temperature, a single T_1 minimum and a parabolic dependence of log T_1 on the temperature is expected. The situation changes if τ exhibits a non-Arrhenius behavior, for example due to tunneling. In this situation, Eq. (91) can to be used to determine the exchange rates from the T_1 rates, if the position and value of the T_1 minimum is known. Figure 10 compares, as an example, the normal Arrhenius T_1 curve to a non-Arrhenius T_1 curve, due to tunneling.

3.4.8. Subspace Structure of the Liouville Space

One major problem in the simulation of the influence of the incoherent exchange rates on the ^{2}H NMR spectra is that, due to the size of the Liouville operator, the necessary numerical simulation of the spectra is very time consuming and renders it impossible to fit experimental spectra in a reasonable time. Realizing that the matrix representation of the $\hat{\hat{M}}$ superoperator is highly sparse, we started to analyze the subspace structure of the Liouville space. We found that $\hat{\hat{M}}$ can be transferred into a block diagonal form, where all the evolution of the measurable magnetization takes place in four two dimensional $\{\mathbf{L}_1, \mathbf{L}_2, \mathbf{L}_3, \mathbf{L}_6\}$ and two four dimensional subspaces $\{\mathbf{L}_4, \mathbf{L}_5\}$ of the Liouville space, which are spanned by the following sets of base vectors:

$$\mathbf{L}_1 = \left\{ \begin{matrix} | & 0 & - & - & - &) \\ | & - & 0 & - & - &) \end{matrix} \right\} \mathbf{L}_2 = \left\{ \begin{matrix} | & 0 & + & + & + &) \\ | & + & 0 & + & + &) \end{matrix} \right\}$$
$$\mathbf{L}_3 = \left\{ \begin{matrix} | & 0 & 0 & - & 0 &) \\ | & 0 & 0 & 0 & - &) \end{matrix} \right\} \mathbf{L}_6 = \left\{ \begin{matrix} | & + & + & 0 & + &) \\ | & + & + & + & 0 &) \end{matrix} \right\} \tag{97}$$

$$\mathbf{L}_4 = \left\{ \begin{matrix} | & - & + & 0 & - &) \\ | & - & + & - & 0 &) \\ | & + & - & 0 & - &) \\ | & + & - & - & 0 &) \end{matrix} \right\} \mathbf{L}_5 = \left\{ \begin{matrix} | & 0 & + & + & - &) \\ | & + & 0 & + & - &) \\ | & 0 & + & - & + &) \\ | & + & 0 & - & + &) \end{matrix} \right\} \tag{98}$$

The resulting two dimensional suboperators $\hat{\hat{M}}_k$ are:

$$\hat{\hat{M}}_1 \begin{pmatrix} -k + 2\pi i(q_1 + X_{12}) & k - 2\pi i X_{12} \\ k - 2\pi i X_{12} & -k + 2\pi i(q_2 + X_{12}) \end{pmatrix} \tag{99}$$

$$\hat{\hat{M}}_2 \begin{pmatrix} -k + 2\pi i(-q_1 + X_{12}) & k - 2\pi i X_{12} \\ k - 2\pi i X_{12} & -k + 2\pi i(-q_2 + X_{12}) \end{pmatrix} \tag{100}$$

$$\hat{\hat{M}}_3 \begin{pmatrix} -k + 2\pi i(q_1 - X_{12}) & k - 2\pi i X_{12} \\ k - 2\pi i X_{12} & -k + 2\pi i(q_2 - X_{12}) \end{pmatrix}$$

and

$$\hat{\hat{M}}_6 \begin{pmatrix} -k - 2\pi i(q_1 + X_{12}) & k - 2\pi i X_{12} \\ k - 2\pi i X_{12} & -k - 2\pi i(q_2 + X_{12}) \end{pmatrix}.$$

The four dimensional suboperators are:

$$\hat{\hat{M}}_4 \begin{pmatrix} -k - 2\pi i q_1 & 2\pi i X_{12} & -2\pi i X_{12} & k \\ 2\pi i X_{12} & -k - 2\pi i q_2 & k & -2\pi i X_{12} \\ -2\pi i X_{12} & k & -k - 2\pi i q_1 & 2\pi i X_{12} \\ k & -2\pi i X_{12} & 2\pi i X_{12} & -k - 2\pi i q_2 \end{pmatrix} \tag{101}$$

and

$$\hat{\hat{M}}_5 \begin{pmatrix} -k + 2\pi i q_1 & -2\pi i X_{12} & 2\pi i X_{12} & k \\ -2\pi i X_{12} & -k + 2\pi i q_2 & k & 2\pi i X_{12} \\ 2\pi i X_{12} & k & -k + 2\pi i q_1 & -2\pi i X_{12} \\ k & 2\pi i X_{12} & -2\pi i X_{12} & -k + 2\pi i q_2 \end{pmatrix}. \tag{102}$$

3.5. Numerical Simulations of ^{2}H NMR Quantum Dynamics in Transition Metal

In the calculations the initial condition is that a 90° pulse was applied to the spin system in thermal equilibrium and thus the initial density matrix $|\rho(0))$ is given by $|F_x)$:

$$|\rho_0) = |F_x) = |I_{1x}) + |I_{2x}) \tag{103}$$

In all cases a grid of 128×128 equally spaced polar angles was employed for calculating the powder integrals. The calculations are performed either in the full Liouville space or alternatively (simulations of experiment) in the subspaces shown above. In the latter case the dynamic superoperator is transformed into these subspaces and the spectra are calculated by diagonalization of the $\hat{\hat{M}}_k$ superoperators in these subspaces and transformation of the $|F_{+k})$ operators into the eigenbase of the $\hat{\hat{M}}_k$. In the simulations for both deuterons, an axial symmetric quadrupolar tensor ($\eta = 0$) with $q_{zz} = 70$ kHz, which was estimated from the room temperature spectra of the Ru-D_2, was used. The spectra were calculated for different relative orientations 2β of the two tensors, varying from $2\beta = 0°$ to $\beta = 90°$. Since for $2\beta = 0°$ the quadrupolar tensors of the two deuterons are collinear, the spectra (not shown) are neither influenced by coherent nor incoherent exchange.

3.5.1. Single Crystals

For purely incoherent exchange, the spectra exhibit the typical incoherent exchange scenario (not shown), which is well known from text books:[70] line broadening of the NMR lines for small exchange rates; line coalescence at exchange rates on the order of the difference of the quadrupolar splitting; again line narrowing at fast exchange rates; full motional averaging of the difference of the quadrupolar splitting in the spectrum at very fast exchange rates.

Figure 11 shows the effects of purely coherent tunneling on the spectra for three different relative orientations of the quadrupolar tensors. The external magnetic field is chosen parallel to the principal axis corresponding to the z-component of the quadrupolar tensor of deuteron 1. Only the spectra calculated with $2\beta = 0°$ are not affected by the exchange. This can be easily understood by realizing that in this case the system is degenerated and both deuterons have the same quadrupolar frequency. For all other angles the spectra exhibit a distinctively different behavior. For small coherent exchange frequencies a splitting of the lines into doublets is observed which increases with the coherent exchange frequency.

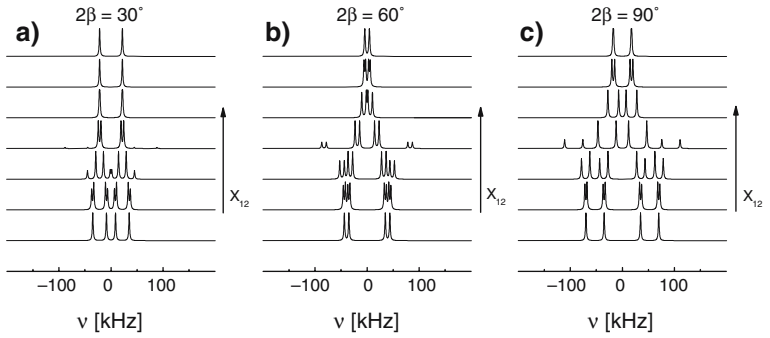

Fig. 11. Simulation of coherent exchange (tunneling) in the ^{2}H NMR spectra of a single crystal for 3 different relative orientations of the two quadrupolar tensors. The external magnetic field is parallel to the principal axis corresponding to q_{zz} of the first tensor. $q_{zz} = 70\,\text{kHz}$, $\eta = 0$, $k_{12} = 0$, 2, 32, 128, 512, and 2048, 8192 kHz. In contrast to the incoherent exchange, the spectra exhibit a splitting instead of a broadening. The spectrum for $X_{12} \gg q$ is identical to the fast incoherent exchange spectrum.

For coherent exchange frequencies on the order of the quadrupolar splitting the intensity ratio of the lines changes and typical higher order NMR spectra are observed, where the main line intensities are at the inner transitions. Moreover, the splitting of the inner pair of lines narrows, while the splitting of the outer lines increases with the coherent exchange frequency. Finally, for coherent exchange frequencies much larger than the difference of the quadrupolar coupling constants, once more a simple two-line spectrum is observed which is identical with the corresponding spectrum for incoherent exchange. The differences between coherent exchange and incoherent exchange are most pronounced for rates on the order of the quadrupolar splitting. The incoherent exchange broadens the lines so strongly that their relative amplitude compared to the amplitude of the spectra for low or high rates is close to zero in the coalescence regime. The coherent tunneling, however, leads to splitting of the lines into doublets, and in particular the relative amplitude of the central lines is only weakly affected by the tunneling

Figure 12 displays the effect of the simultaneous presence of coherent and incoherent exchange. While for the lowest coherent exchange frequency the effect of incoherent exchange is immediately visible in the spectra, for increasing coherent exchange frequency the incoherent exchange rate has to be increased to have a visible effect on the spectra. In particular the broadening of the lines starts for incoherent exchange rates on the order of the coherent exchange frequency, while for incoherent exchange rates far below the coherent frequency, the effects of the inco-

herent exchange are not visible. In other words, the shape of the spectra is determined by the relative speed of coherent versus incoherent exchange. Moreover this faster rate must be at least on the order of the difference of the quadrupolar splitting to have an effect on the spectra.

3.5.2. Non-oriented Powder Samples

The upper part of Fig. 13 depicts the effects of incoherent exchange of the two deuterons as a function of the rotation angle 2β for randomly oriented powder samples. As in the case of single crystals the effect of the incoherent exchange is most pronounced for $2\beta = 90^\circ$. The exchange first causes a smearing of the edges of the Pake pattern and then the typical formation of a narrowed Pake pattern, whose asymmetry parameter depends on the angle between the two tensors.

The lower part of Fig. 13 displays the results of the same calculations for the case of coherent exchange of the two different deuterons. While for small or large coherent exchange frequency these spectra are practically indistinguishable from the spectra of incoherent exchange, there are pronounced differences for intermediate spectra, where the coherent exchange frequency is on the order of the quadrupolar coupling. For these spectra, the satellite transitions, which have appeared in the single crystal spectra, lead to spectral contributions outside the range of the spectra without coherent exchange. Moreover in this intermediate range, the singularities in the spectra appear much sharper than the singularities in the corresponding incoherent exchange spectra.

Figure 14 finally shows the calculation of powder spectra, where both coherent and incoherent exchange are simultaneously present. Again the relative size of the coherent tunneling frequency versus incoherent exchange rate determines the shape of the NMR spectra. If the coherent exchange frequency is small, i.e. ($X_{12} \ll Q$), the spectra exhibit exactly the same behavior as the spectra without coherent exchange. On the other hand, for a fast coherent exchange ($X_{12} \gg Q$), the effect of the incoherent exchange on the spectra is invisible. In the intermediate regime ($X_{12} \approx Q$), the spectra exhibit a rather complicated line shape, which nevertheless still shows the sharp features of the coherent tunneling line shape. Again, for all coherent exchange frequencies, the spectra at fast incoherent rates are identical and only for intermediate exchange rates an effect on the spectra is visible.

Thus there are pronounced differences between coherent and incoherent exchange of two deuterons in the ^{2}H NMR spectra of these deuterons: The former lead to a splitting of the spectral lines and the latter lead first to a broadening and later to a narrowing of the lines. This is the experi-

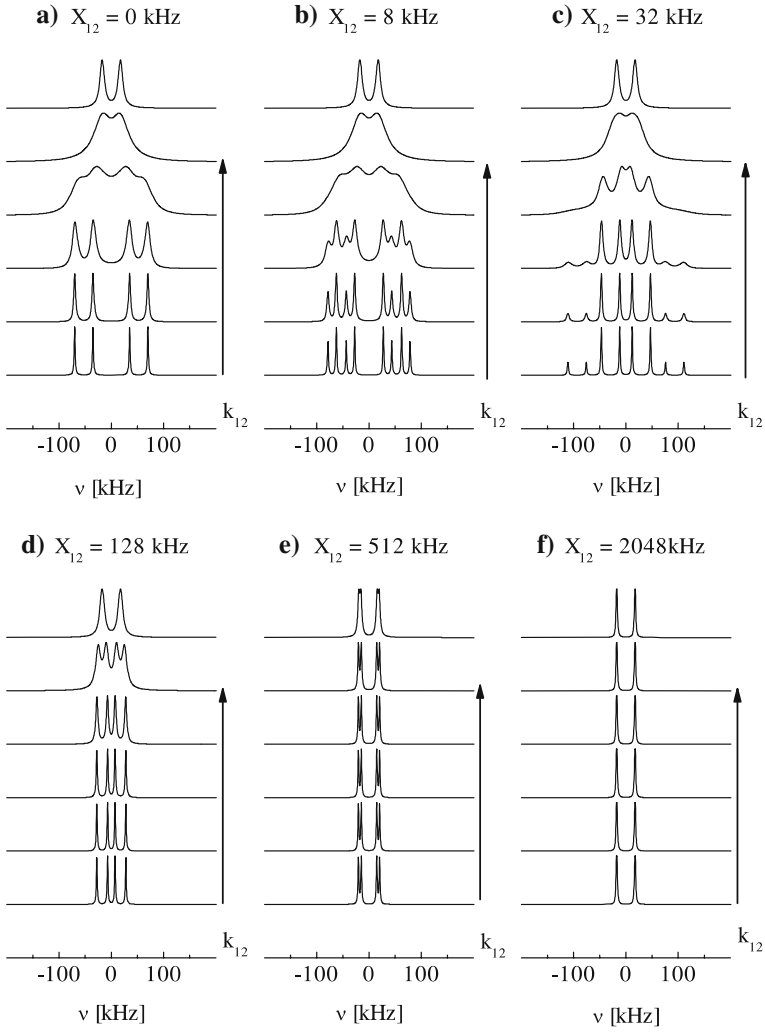

Fig. 12. Simulation of simultaneous incoherent k_{12} and coherent X_{12} exchange (tunneling) in single crystals: $q_{zz} = 70\,\text{kHz}$, $\eta = 0$, $k_{12} = 0$, 8, 32, 128, 512, and 2048 kHz. The external magnetic field is parallel to the principal axis corresponding to q_{zz} of the first tensor. The second tensor is rotated with $2\beta = 90^\circ$ with respect to the first tensor. The relative size of coherent and incoherent exchange rates determines the shape of the spectral lines.

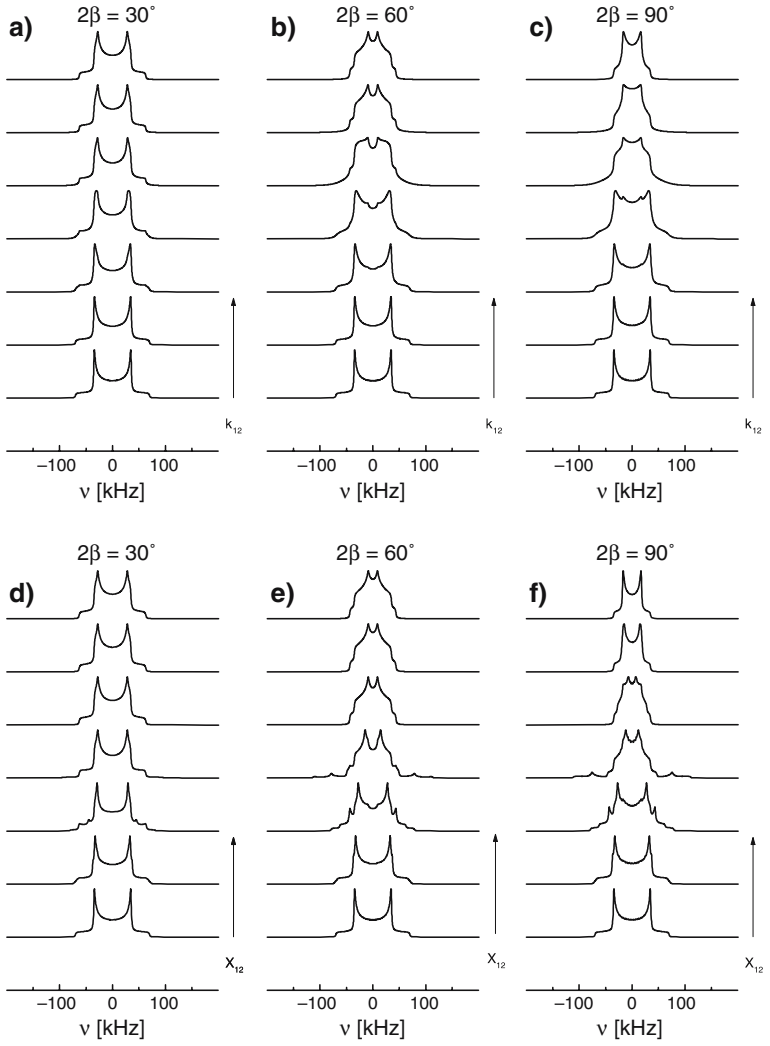

Fig. 13. Comparison of the effects of coherent tunneling and incoherent exchange on the ^{2}HNMR spectra of a non-oriented powder sample (powder spectra) for three different relative orientations of the quadrupolar tensors. Upper row: Simulation of incoherent exchange. $q_{zz} = 70\,\text{kHz}$, $\eta = 0$, $k_{12} = 0$, 2, 32, 128, 512, 2048, and 8192 kHz. The incoherent exchange mainly leads to a smearing of the edges of the Pake pattern, which for higher rates narrows to the average spectrum. Lower row: Simulation of coherent tunneling: $q_{zz} = 70\,\text{kHz}$, $\eta = 0$, $X_{12} = 0$, 2, 32, 128, 512, 2048, and 8192 kHz. In the intermediate range of coherent exchange frequencies there are satellite lines, which clearly distinguish the spectra from the corresponding incoherent spectra.

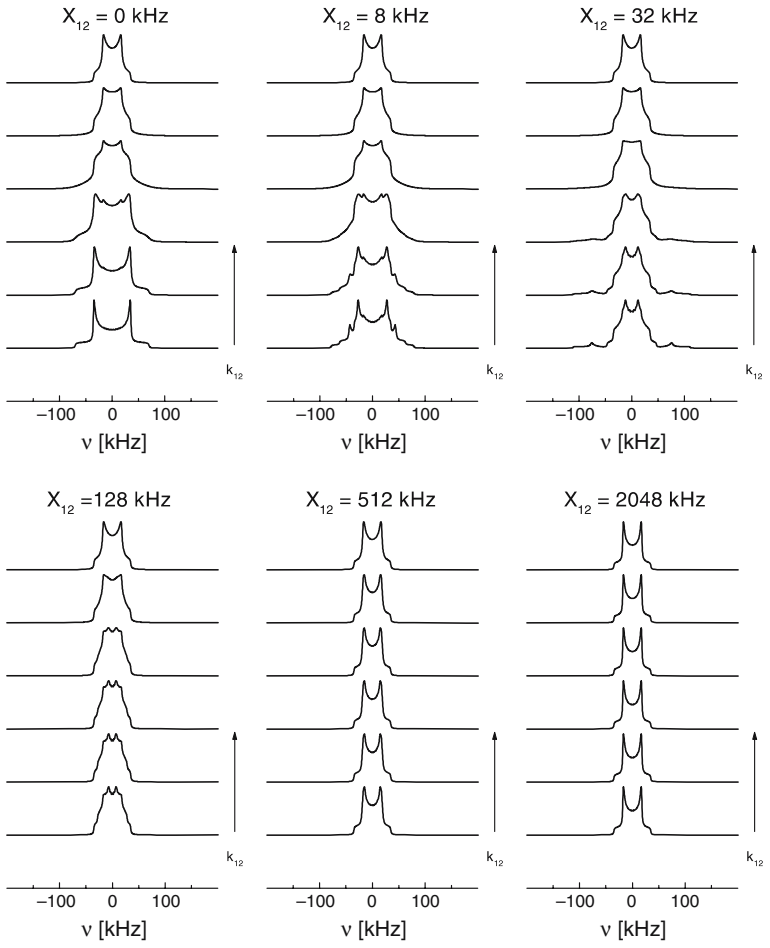

Fig. 14. Simulation of simultaneous incoherent and coherent exchange (tunneling) for the same relative orientations and parameters: $2\beta = 90^\circ$, $q_{zz} = 70$ kHz, $\eta = 0$, $k_{12} = 0$, 8, 32, 128, 512, and 2048 kHz as above. The relative size of coherent and incoherent exchange rates determines the shape of the spectral lines. Note in particular that for X_{12} or $k_{12} \gg q$, the shape of the spectra is independent on the second kind of exchange process.

mental manifestation of the result from the theoretical description that the exchange can be interpreted as a relaxation of coherences between states of different symmetry with respect to particle permutation.

These differences are most pronounced for coherent exchange frequencies which are on the order of the quadrupolar coupling constant. Thus by investigation of this range of intermediate tunnel splitting, it

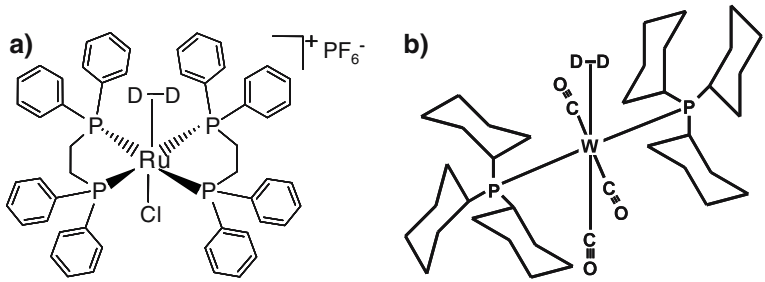

Fig. 15. Left: Structure of the Ru-D_2 complex *trans*-[Ru(D_2)Cl(dppe)$_2$]PF_6. Right: Structure of the tungsten (W-D_2) complex W(PCy_3)$_2$(CO)$_3$($\eta^2 - D_2$), also known as the Kubas complex.

is possible to distinguish not only between coherent and incoherent exchange, but also to determine the size of the tunnel splitting. The actual effect on the spectra depends strongly on the relative orientation of the quadrupolar tensors associated with the two deuterons. If these tensors are collinear, the spectra are neither affected by coherent nor by incoherent exchange. If, on the other hand, the two tensors are rotated 90° relative to each other, the effect is most pronounced.

4. EXPERIMENTAL EXAMPLES

4.1. Samples

Two different selectively D_2 labeled transition metal complexes were studied as model systems for the study of coherent and incoherent D_2 dynamics, namely a *trans*-[Ru(D_2)Cl(dppe)$_2$]PF_6 complex (Ru-D_2) and the Kubas (W-D_2) complex W(PCy_3)$_2$(CO)$_3$(η^2-D_2).[23] The main difference, concerning their dynamic properties, is the expected height of the barrier, which hinders the free rotation of the two deuterons.

The η^2-bond complex Ru-D_2 (see Fig. 15) was chosen because of its high stability, the absence of isotope scrambling (i.e. unwanted deuterium incorporation into C–H bonds) and its estimated ^{1}H–^{1}H distance of 0.99Å,[28] which is an indication for a relatively high rotational barrier with tunnel splitting in the proper range of ^{2}H-solid state NMR.

The protonated isotopomer W-H_2 of the W-D_2 complex had already been studied by INS spectroscopy.[16] In this study a relatively low tunneling barrier of 7 kJ/mol (73 meV) was estimated from the splitting of the INS line. This barrier height is about a factor of 4 smaller than the expected barrier height of the Ru-D_2 sample, making the Kubas complex an ideal sample for the search of ^{1}H–^{2}H isotope effects on the tunneling.

Details of the synthesis and sample preparation are found in the original papers.[23,39,40]

4.2. Coherent D_2 and Incoherent Rotational D_2 Tunneling in the Ru-D_2 Sample

From the numerical estimations of tunnel splitting visible by NMR shown above, it is evident that only at temperatures below ≈ 20 K there exists a reasonable chance of observing the tunnel splitting, because at higher temperatures the incoherent processes will determine the spectral line shape. Therefore all experiments were performed in a helium cooled low temperature cryostat. In this cryostat system the ^{2}H NMR spectra and T_1 relaxation of the complex are studied. Most of these results are published in reference.[39]

Figure 16 compares experimental ^{2}H-solid echo NMR spectra and the simulated ^{2}H-FID-NMR spectra of the Ru-D_2 complex. In the temperature range between 20 and 230 K the ^{2}H NMR line corresponds to a typical ^{2}H NMR quadrupolar pattern with an asymmetry of $\eta = 0.2$. The width of the line decreases slowly with increasing temperature. At temperatures above 230 K an additional narrow component appears in the center of the spectrum. Below 20 K a strong increase of the spectral line width is observed. Moreover a satellite Pake pattern appears with its singularities at frequencies of ± 60 kHz. The position of these singularities increases weakly with the temperature. The line width of these singularities, which is rather small at 5.4 K, increases strongly with increasing temperature until they have disappeared at 22.8 K.

Figure 17 displays the result of the T_1 measurements on the Ru-D_2 complex. Due to the low sensitivity of the sample the spin–lattice relaxation rates were measured only at some selected temperatures. The lowest T_1 value (0.12 ± 0.02 s) was found at 97 K. At low temperatures the T_1 data show strong deviations from a simple Arrhenius behavior.

In the next step the attribution of the satellite Pake pattern in the ^{2}H NMR spectra of this Ru-D_2 complex given in reference[39] is summarized. From the sample preparation a chemical impurity can be excluded. Molecular polymorphism with two different conformers can be excluded by the low temperature where the satellites exist. Chemical shielding, J-coupling and homonuclear dipolar D–D or heteronuclear Ru-D, ^{31}P-D or ^{1}H-D dipolar interactions are to weak for the size of the observed splitting. Thus it follows that the splitting below 20 K has to be attributed to the proposed quantum mechanical exchange mechanism.

Using the theoretical model, the experimental spectra were simulated assuming a superposition of a coherent and an incoherent exchange pro-

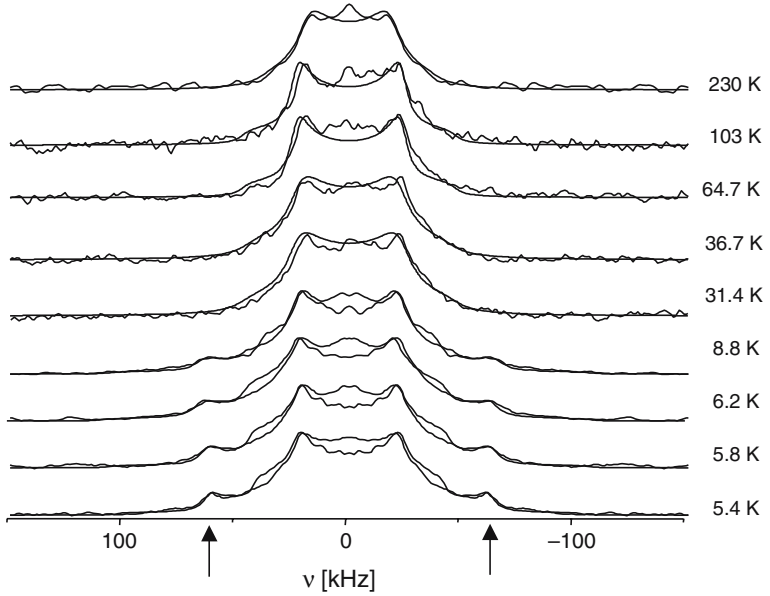

Fig. 16. Experimental and simulated ^{2}H NMR Spectra of the Ru-D_2 complex, measured in the temperature range from 5.4 to 230 K. At temperatures below 8.8 K, a splitting in the ^{2}H-NMR line shape is clearly visible (arrows). This splitting can be explained by a coherent tunneling of the two deuterons in the Ru-D_2 sample (simulation as ^{2}H-FID-NMR experiment). The simulations were performed with $q_{zz} = 80 \pm 3$ kHz (i.e. $q_{cc} = 107 \pm 4$ kHz), $\eta = 0$ and a jump angle between the two tensor orientations of $2\beta = 90^\circ$.

cess. The actual simulations were done by Fourier-transforming the FIDs calculated from Eqs. 100 to 103 instead of calculating the solid echo spectra under the influence of these interactions. The latter is numerically orders of magnitude more complex and to slow for a fitting of the data. In principle this procedure introduces an error in the line shape for incoherent exchange rates in the intermediate motional regime. Tentative simulation of incoherent two-fold exchange with the parameters of the experimental data show that the overall differences in the line shape are not significant, compared to the signal/noise ratio of the spectra. Until now no calculations of the solid echo spectra under the influence of both coherent and incoherent exchange have been performed for reasons of numerical effort.

From the exchange model the following data are extracted: the angle between the tensor orientations, the coherent tunnel rate X_{12} and the incoherent exchange rate k_{12}. The coherent tunnel rate X_{12} varies only weakly and the incoherent exchange rate k_{12} varies strongly as a function

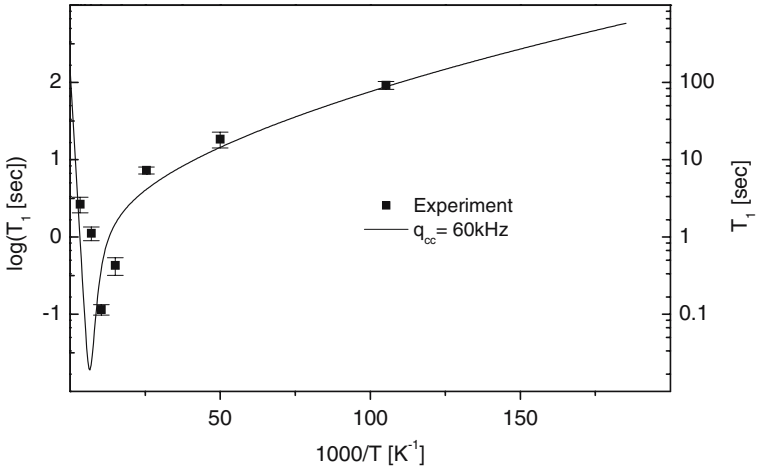

Fig. 17. T_1 relaxation data of the Ru-D_2 complex: Experimental points from line shape analysis and relaxation measurements. The solid line is calculated from the exchange rates calculated from the modified Bell model using the value of $K^{\mathrm{EFG}} = 0.3\pi^2(60\,\mathrm{kHz})^2$.

of the temperature. The quadrupolar coupling and the angle between the principal axes of the two quadrupolar tensors were adapted from the simulations of the low temperature spectrum at 5.4 K and the high temperature spectrum at 320 K, assuming that the latter corresponds to the fast exchange limit. The best fit was obtained using an angle of $2\beta = (90 \pm 10)^\circ$ between the PAS and a nearly axial symmetric ($\eta < 0.1$) quadrupolar tensor with $q_{zz} = (80 \pm 3)$ kHz.

The difference of the jump angle of $90^\circ \pm 10^\circ$ to the bond angle of 34° is a result of the η^2-dihydrogen state, where the electron density is both between the metal and the deuterons and between the deuterons (see Fig. 18).

Figure 19 shows an Arrhenius plot of the temperature dependence of X_{12} and k_{12} extracted from the ^{2}H NMR spectra and relaxation measurements. The temperature dependence of X_{12} is very weak and nearly linear in the temperature window between 5 and 20 K and can be approximated as (dashed line):

$$X_{12} = 26.7\,\mathrm{kHz} - 0.038\,\mathrm{kHz}\cdot\mathrm{K} \times 1000/T \tag{104}$$

Assuming the simple harmonic potential of Eq. (1) the height of the rotational barrier can be estimated. Using the value of $R_{\mathrm{HH}} = 1$ Å, a rotational barrier of $2V_0 = 270$ meV (6.22 kcal/mol) is calculated.

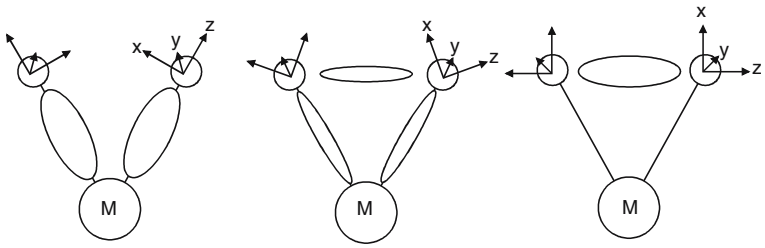

Fig. 18. Quadrupolar tensor orientations: Sketch of the electron density distribution and the orientations of the quadrupolar tensors for a dihydride (left), η-bond (center) and a dihydrogen complex (right).

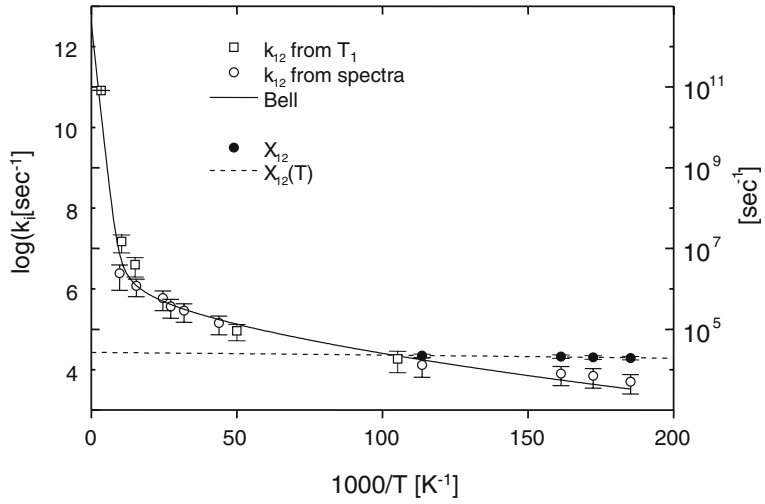

Fig. 19. Arrhenius plot of the temperature dependence of the coherent tunneling and incoherent exchange rates in the Ru-D_2 sample, extracted from Figs. 16 and 17. The solid line is the result of a fit of the temperature dependence of the incoherent rates using a modified Bell tunnel model (see text). The dashed line is a simple linear fit of the coherent tunnel rates.

The exchange rates from the relaxation data are obtained for $K^{\mathrm{EFG}} = 0.3\pi^2\ (60\,\mathrm{kHz})^2$ and the rate data from the spectra by line shape analysis. The incoherent rates k_{12} exhibit much stronger temperature dependence, varying from $5 \times 10^3\,\mathrm{s}^{-1}$ at 5.4 K to ca. $2.5 \times 10^6\,\mathrm{s}^{-1}$ at 103 K and ca. $10^{11}\,\mathrm{s}^{-1}$ at 300 K. The rate data from both types of experiments overlap between 20 and 100 K and there is an excellent agreement between the values. This indicates that both rates result from the same motional process.

The simulation of the temperature dependence was performed assuming a thermally activated tunneling process, described by a Bell type of tunneling. The high temperature rate in the tunnel model was chosen as $4 \times 10^{12}\,s^{-1}$, which is expected from the Eyring equation. The observed increase of k_{12} at low temperatures is not obtainable by the simple one dimensional Bell model. This shows that a complete description of the temperature dependence of the rates needs at least a two dimensional model, where the average R_{HH} and/or R_{RuH} distances are functions of the temperature. In a simple one dimensional model, a temperature dependent effective tunnel barrier was employed, where the effective potential is a power law function of the temperature:

$$V_{eff}(T^{-1}) = V(T_0^{-1}) + (V(T_1^{-1}) - V(T_0^{-1}))\left(\frac{T^{-1} - T_0^{-1}}{T_1^{-1} - T_0^{-1}}\right)^G \qquad (105)$$

The best fit of the experimental rates (solid line in Fig. 19) was found for an exponent of $G = 0.7$, i.e. for a relatively linear temperature variation of the effective potential, varying between 268 meV(6.18 kcal/mol) at 5.4 K and 129 meV (2.97 kcal/mol) at 300 K. This effective potential gives a good reproduction of the experimental data. These rates were used to calculate the whole T_1 dependence (solid line in Fig. 17).

Comparing the values of the quadrupolar coupling constant obtained from the line shape analysis with the $K^{EFG} = 0.3\pi^2\ (60\,kHz)^2$ value from the relaxation data it is evident, that K^{EFG} is in between the values expected for rotational diffusion and jump diffusion, which can be considered as the limiting cases of the motions responsible for the relaxation. It follows that the motional process responsible for the relaxation is somewhere in between the pure two site jump of Eq. (94) and the free rotational diffusion of Eqs. (93) and (95). Such a mechanism could be a combination of torsional vibrations with the jump process or four-fold distortions of the simple twofold potential of Eq. (1).

4.3. Isotope Effects on Dihydrogen-Dynamics of the Kubas Complex

This section studies isotope effects on the dihydrogen dynamics obtained on the Kubas complex, by comparing dynamic data from ^{2}H-spin–lattice relaxation of the deuterated (W-D_2) complex to INS data of the protonated (W-H_2) complex. Experimental details are found in Wehrmann *et al.*[40] Figure 20 presents the experimental ^{2}H NMR spectra of the W-D_2 complex, together with simulations of the spectra (see discussion below). The ^{2}H NMR spectrum consists mainly of two spectral components. The major intensity is concentrated in a rather unusual Pake like

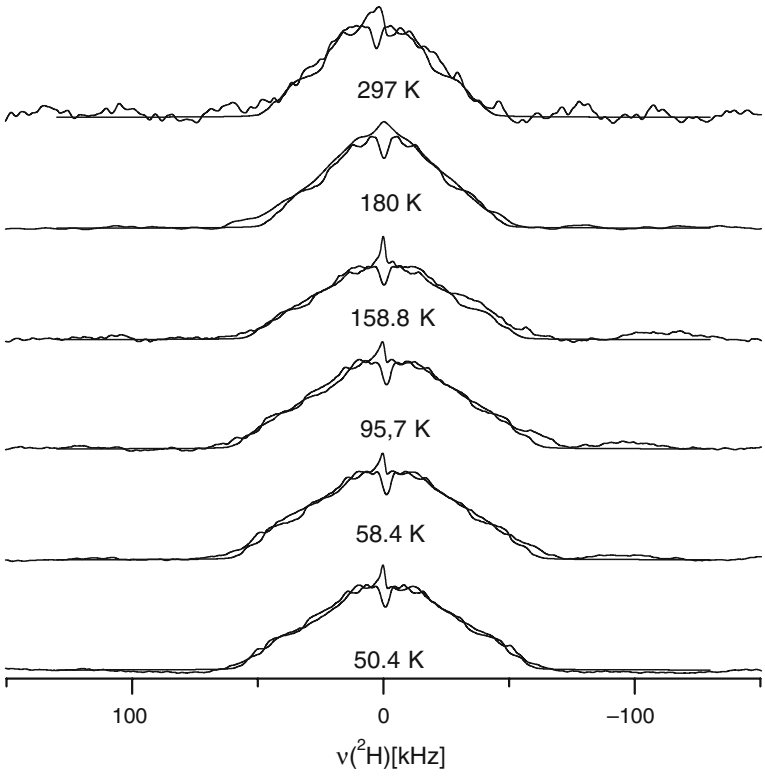

Fig. 20. Experimental and simulated ^{2}H NMR spectra of the W-D_2 complex at different temperatures. Simulation as a superposition of a quadrupolar pattern and a homonuclear dipolar D–D interaction of 4 kHz, corresponding to a D–D distance of 0.89 Å.

pattern with an asymmetry factor of $\eta = 0.62$ and a temperature dependent quadrupolar interaction, which decreases slowly from a value of 55 kHz at 50 K to a value of 40 kHz at 180 K. With the exception of this small decrease of the quadrupolar interaction, the ^{2}H NMR spectrum is nearly temperature independent in the range between 50 and 300 K. In addition to the Pake like component, a narrow component, which accounts for less than 5% of the spectral intensity is present in the center of the spectrum at all temperatures. Since the sealed sample is filled with a D_2 atmosphere, which is in slow exchange with the η^2-bound deuterium of the complex, we attribute this narrow component to this gaseous and/or physisorbed D_2 molecules, which are highly mobile.

A detailed discussion in the original paper[40] shows that the spectra have to be attributed to a superposition of the quadrupolar and an addi-

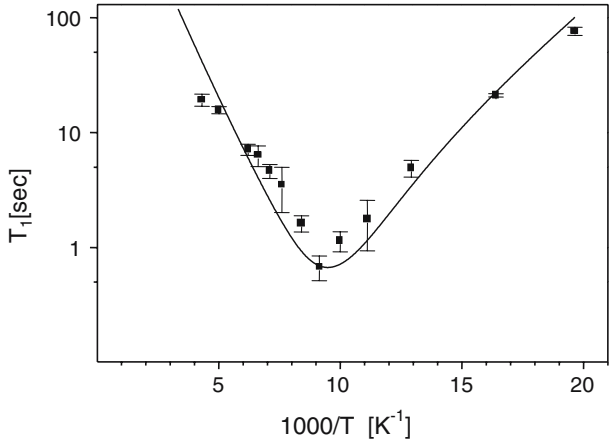

Fig. 21. Experimental temperature dependence of the ^{2}H-spin–lattice relaxation in the W-D_2 complex. The data exhibit deviations from the Arrhenius behavior at low temperatures. The solid line is calculated from the exchange rates calculated from the Bell model.

tional homonuclear dipolar interaction. From the simulation the quadrupolar coupling constant at low temperatures is $q_{cc} = 4/3 \cdot 55\,\text{kHz} = 73\,\text{kHz}$ and the homonuclear dipolar interaction is 4 ± 1 kHz (corresponding to a D–D distance of 0.89 ± 0.1 Å). The latter value is in good agreement with the value of 0.89 Å reported for the protonated complex in literature.[98,107]

Figure 21 presents the experimental results of the temperature dependence of the ^{2}H NMR spin–lattice relaxation time measurements on the W-D_2 sample together with a calculation of the relaxation times (see below). The T_1 measurements in the temperature regime from 50 K to 230 K show a strong temperature dependence of T_1 with a sharp minimum close to 110 K. At the minimum a T_1 relaxation time of (0.68 ± 0.15) sec is found. It is evident that in the low temperature branch of the spin–lattice relaxation curve there are deviations from a simple Arrhenius behavior, visible in a flattening of the curve.

The interpretation of the T_1 minimum shows that jump mechanism is the most probable origin of the T_1 relaxation. In this case a value of $q_{cc} = 68$ kHz is found, which agrees well with the quadrupolar coupling constant visible in the ^{2}H NMR spectra at low temperatures ($q_{cc} = 4/3 \cdot 55\,\text{kHz} = 73\,\text{kHz}$).

Employing Eqs. (92) and (96), the T_1 values can be converted to rate constants of the D–D exchange. The resulting curve (Fig. 22) shows a deviation from a simple Arrhenius behavior at low temperatures. This deviation is evidence for the presence of a quantum mechanical tunneling

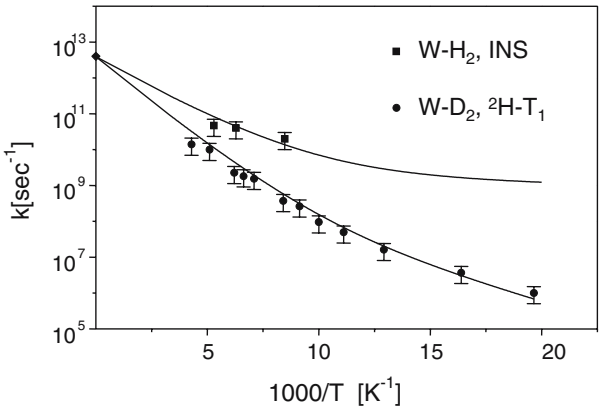

Fig. 22. Arrhenius plot of the temperature dependence of the incoherent exchange rates in the W-D2 sample, extracted from the ^{2}H-T_1 data. The data are compared to data obtained on the W-H_2 complex, determined by incoherent neutron scattering (INS). The solid lines are the results of fits of the temperature dependence of the incoherent rates using a Bell type tunnel model. The fits reveal a strong isotope effect, which is not solely attributable to a simple mass effect. The high temperature limit of the rates was chosen as $4 \times 10^{12}\,s^{-1}$, according to the Eyring equation.

process at low temperatures, similar to the tunneling observed in the Ru-D_2 sample. The comparison of these rate data to the H–H exchange rates determined from the line shape analysis[16] of the INS spectra of the protonated species reveals a strong isotope effect, which increases with lower temperatures.

Calculations with the Bell tunnel model reveal that this isotope effect is not solely explainable by the differences of the masses of the two hydrogen isotopes, but that also the activation energy must have changed. This difference in the height of the activation barrier can be caused by two reasons, which are not necessarily mutually exclusive, namely isotope effects on the M–D and D–D versus M–H and H–H distances or by difference in the zero point energy of the ground or an activated state, which serves as the transition state for the tunneling. Since the width of the spectra and thus the quadrupolar interaction is temperature independent at temperatures below 150 K one can conclude that the W-D_2 distance is more or less constant at low temperatures and that the differences in the zero point or transition state energies are the major contribution to the isotope effect.

5. SUMMARY AND CONCLUSION

^{2}H NMR has been exploited for the analysis of the structure and dynamics of η^2-bound dideuterium transition metal complexes. A complete Alexander–Binsch representation of the NMR theory of a system of two deuterons under the influence of quadrupolar interaction, mutual incoherent exchange and quantum mechanical tunneling has been developed and analyzed analytically and numerically. It is shown that the superoperator, which determines the dynamics of the spin system, can be transferred into a block diagonal form, where all the evolution of the measurable magnetization takes place in four two-dimensional and two four-dimensional subspaces of the Liouville space, leading to a drastic simplification of the numerical calculation of the exchange effects. Employing a helium-cooled low-temperature ^{2}H NMR setup with highly sensitive ^{2}H NMR probes, we succeeded for the first time in the experimental observation of coherent tunneling of a D_2-pair in the solid state. The compound studied was a Ru-D_2 complex, for which a relatively high rotational barrier was expected. The temperature dependence of the deuteron dynamics in the range of 5–300 K has been analyzed for this system by a combination of ^{2}H line shape analysis and T_1 relaxation measurements. In a second transition metal dideuteride, namely a W-D_2 complex, we found by comparison of ^{2}H-T_1 relaxation data to INS data experimental evidence for a strong ^{1}H–^{2}H isotope effect on the incoherent exchange rates.

These results have strong implications for the analysis of the ^{2}H–solid state NMR spectra of catalytic active transition metal nano particles, where similar effects are observed[108] and the basic mechanism of *ortho–para* conversion of *para*-Hydrogen on metal surfaces,[109,110] since also in these cases in the course of the initial chemisorption of the hydrogen, these intermediate dihydrogen states are passed.

ACKNOWLEDGMENT

Financial support by the Deutsche Forschungsgemeinschaft (DFG) is gratefully acknowledged.

REFERENCES

1. N. Aebischer, U. Frey, and A. E. Merbach, *Chem. Comm.* 2303 (1998).
2. G. Albertin, S. Antoniutti, S. Garciafontan, R. Carballo, and F. Padoan, *J. Chem. Soc., Dalton Trans*. 2071 (1998).
3. I. Alkorta, I. Rozas, and J. Elguero, *Chem. Soc. Rev*. **27**, 163 (1998).
4. V. I. Bakhmutov, *Inorg. Chem*. **37**, 279 (1998).
5. T. Y. Bartucz, A. Golombek, A. J. Lough, P. A. Maltby, R. H. Morris, R. Ramachandran, and M. Schlaf, *Inorg. Chem*. **37**, 1555 (1998).

6. M. G. Basallote, J. Duran, M. J. Fernandez-Trujillo, and M. A. Manez, *J. Chem. Soc., DaltonTrans*, 2205 (1998).
7. C. Bohanna, B. Callejas, A. J. Edwards, M. A. Esteruelas, F. J. Lahoz, L. A. Oro, N. Ruiz, and C. Valero, *Organometallics* 373 (1998).
8. G. Buntkowsky, H.-H. Limbach, F. Wehrmann, I. Sack, H. M. Vieth, and R. H. Morris, *J. Phys. Chem. A* **101**, 4679 (1997).
9. B. Chaudret, *Coord. Chem. Rev*. **180**, 381 (1998).
10. A. C. Cooper and K. G. Caulton, *Inorg. Chem*. **37**, 5938 (1998).
11. R. H. Crabtree, *J. Organomet. Chem*. **557**, 111 (1998).
12. M. A. Esteruelas and L. A. Oro, *Chem. Rev*. **98**, 577 (1998).
13. R. Gelabert, M. Moreno, J. M. Lluch, and A. Lledos, J. Am. Chem. Soc. **120**, 8168 (1998).
14. S. Gründemann, H.-H. Limbach, V. Rodriguez, B. Donnadieu, S. Sabo-Etienne, and B. Chaudret, *Ber. Bunsenges. Phys. Chem.* **102**, 344 (1998).
15. T. Hasegawa, Z. W. Li, and H. Taube, *Chem. Lett*. 7 (1998).
16. H.-H. Limbach, S. Ulrich, S. Gründemann, G. Buntkowsky, S. Sabo-Etienne, B. Chaudret, G. J. Kubas, and J. Eckert, *J. Am. Chem. Soc*. **120**, 7929 (1998).
17. K. S. Macfarlane, I. S. Thorburn, P. W. Cyr, D. Chau, S. J. Rettig, and B. R. James, *Inorg. Chim. Acta.* **270**, 130 (1998).
18. W. S. Ng, G. C. Jia, M. Y. Huang, C. P. Lau, K. Y. Wong, and L. B. Wen, *Organometallics* **17**, 4556 (1998).
19. P. L. A. Popelier, *J. Phys. Chem. A* **102**, 1873 (1998).
20. S. Sabo-Etienne and B. Chaudret, *Chem. Rev*. **98**, 2077 (1998).
21. S. S. Stahl, J. A. Labinger, and J. E. Bercaw, *Inorg. Chem*. **37**, 2422 (1998).
22. G. J. Kubas, R. R. Ryan, B. I. Swanson, P. J. Vergamini, and H. J. Wasserman, *J. Am. Chem. Soc*. **116**, 451 (1984).
23. G. J. Kubas, *J. Acc. Chem. Res*. **21**, 120 (1988).
24. P. G. Jessop and R. H. Morris, *Coord. Chem. Rev*. **121**, 155 (1992).
25. D. M. Heinekey and W. J. Oldham, *J. Chem. Rev*. **93**, 913 (1993).
26. T. A. Luther and D. M. Heinekey, *Inorg. Chem*. **37**, 127 (1998).
27. A. Toupadakis, G. J. Kubas, W. A. King, L. B. Scott, and J. Huhmann-Vincent, *Organometallics* **17**, 5315 (1998).
28. P. A. Maltby, M. Steinbeck, A. J. Lough, R. H. Morris, W. T. Klooster, T. F. Koetzle, and R. C. Srivastava, *J. Am. Chem. Soc*. **118**, 5396 (1996).
29. S. Q. Niu, L. M. Thomson, and M. B. Hall, *J. Am. Chem. Soc*. **121**, 4000 (1998).
30. M. E. Cucullu, S. P. Nolan, T. R. Belderrain, and R. H. Grubbs, *Organometallics* **17**, 1299 (1998).
31. A. J. Lough, R. H. Morris, L. Ricciuto, and T. Schleis, *Inorg. Chim. Acta* **270**, 238 (1998).
32. J. Matthes, S. Grundemann, A. Toner, Y. Guari, B. Donnadieu, J. Spandl, S. Sabo-Etienne, E. Clot, H. H. Limbach, and B. Chaudret, *Organometallics* **23**, 1424 (2004).
33. F. Maseras, A. Lledos, E. Clot, and O. Eisenstein, *Chem. Rev*. **100**, 601 (2000).
34. A. Macchioni, *Chem. Rev*. **105**, 2039 (2005).
35. S. Lachaize, W. Essalah, V. Montiel-Palma, L. Vendier, B. Chaudret, J. C. Barthelat, and S. Sabo-Etienne, *Organometallics* **24**, 2935 (2005).
36. H. H. Limbach, G. Scherer, and M. Maurer, *Angew. Chem*. **104**, 1414 (1992).
37. H. H. Limbach, G. Scherer, M. Maurer, and B. Chaudret, *Angew. Chem., Int. Ed. Engl*. **31**, 1369 (1990).
38. H. H. Limbach, G. Scherer, L. Meschede, F. Aguilar-Parrilla, B. Wehrle, J. Braun, C. Hoelger, H. Benedict, G. Buntkowsky, W. P. Fehlhammer, J. Elguero, J. A. S. Smith, and B. Chaudret, in *Ultrafast Reaction Dynamics and Solvent Effects, Experimental and Theoretical Aspects*, Y.Gauduel, and P.J.Rossky, (eds.), American Inst. of Physics. (1993), P. 225.
39. F. Wehrmann, T. Fong, R. H. Morris, H.-H. Limbach, and G. Buntkowsky, *Phys. Chem. Chem. Phys.* **1**, 4033 (1999).
40. F. Wehrmann, J. Albrecht, E. Gedat, G. J. Kubas, H. H. Limbach, and G. Buntkowsky, *J. Phys. Chem. A* **106**, 2855 (2002).

41. J. Eckert and G. J. Kubas, *J. Phys. Chem*. **97**, 2378 (1993).
42. T. Arliguie, B. Chaudret, J. Devillers, and R. Poilblanc, *C.R. Acad. Sci. Paris, Serie I* **305**, 1523 (1987).
43. D. M. Heinekey, N. G. Payne, and G. K. Schulte, *J. Am. Chem. Soc*. **110**, 2303 (1988).
44. D. M. Heinekey, J. M. Millar, T. F. Koetzle, N. G. Payne, and K. W. Zilm, *J. Am. Chem. Soc*. **112**, 909 (1990).
45. K. W. Zilm, D. M. Heinekey, J. M. Millar, N. G. Payne, and P. Demou, *J. Am. Chem. Soc*. **111**, 3088 (1989).
46. D. Jones, J. A. Labinger, and J. Weitekamp, *J. Am. Chem. Soc*. **111**, 3087 (1989).
47. S. J. Inati and K. W. Zilm, *Phys. Rev. Lett*. **68**, 3273 (1992).
48. M. T. Bautista, K. A. Earl, P. A. Maltby, R. H. Morris, C. T. Schweitzer, and A. Sella, *J. Am. Chem. Soc*. **110**, 7031 (1988).
49. G. A. Facey, T. P. Fong, D. G. Gusev, P. M. MacDonald, R. H. Morris, M. Schlaf, and W. Xu, *Can. J. Chem*. 1899–1910 (1999).
50. G. Buntkowsky, J. Bargon, and H.-H. Limbach, *J. Am. Chem. Soc*. **118**, 867 (1996).
51. S. Alexander, *J. Chem. Phys*. **37**, 971 (1962).
52. G. Binsch, *J. Am. Chem. Soc*. **91**, 1304 (1969).
53. D. A. Kleier and G. Binsch, *J. Magn. Res*. **3**, 146 (1970).
54. S. Szymanski, *J. Chem. Phys*. **104**, 8216 (1996).
55. S. Szymanski, *Annu. Rep. NMR Spectrosc*. **35**, 794 (1998).
56. C. Scheurer, ETH Zürich, Zürich (1998).
57. C. Scheurer, R. Wiedenbruch, R. Meyer, R. R. Ernst, and D. M. Heinekey, *J. Chem. Phys*. **106**, 1 (1997).
58. W. Wu, D. L. Noble, J. R. Owers-Bradley, and A. J. Horsewill, *J. Magn. Reson*. **175**, 210 (2005).
59. Q. Xue, A. J. Horsewill, M. R. Johnson, and H. P. Trommsdorff, *J. Chem. Phys*. **120**, 11107 (2004).
60. S. Nair, R. M. Dimeo, D. A. Neumann, A. J. Horsewill, and M. Tsapatsis, J. Chem. Phys. **121**, 4810 (2004).
61. R. I. Jenkinson, A. Ikram, A. J. Horsewill, and H. P. Trommsdorff, *Chem. Phys*. **294**, 95 (2003).
62. A. J. Horsewill, C. J. McGloin, H. P. Trommsdorff, and M. R. Johnson, Chem. Phys. **291**, 41 (2003).
63. M. R. Johnson, N. H. Jones, A. Geis, A. J. Horsewill, and H. P. Trommsdorff, *J. Chem. Phys*. **116**, 5694 (2002).
64. A. J. Horsewill and Q. Xue, *Phys. Chem. Chem. Phys*. **4**, 5475 (2002).
65. A. J. Horsewill, N. H. Jones, and R. Caciuffo, *Science* **298**, 1171 (2002).
66. A. J. Horsewill, N. H. Jones, and R. Caciuffo, *Science* **291**, 100 (2001).
67. G. E. Pake, *J. Chem. Phys*. **16**, 327 (1948).
68. E. Gedat, A. Schreiber, J. Albrecht, I. Shenderovich, G. Findenegg, H.-H. Limbach, and G. Buntkowsky, *J. Phys. Chem. B*. **106**, 1977 (2002).
69. W. Masierak, T. Emmler, E. Gedat, A. Schreiber, G. H. Findenegg, and G. Buntkowsky, *J. Phys. Chem. B* 18890 (2004).
70. K. Schmidt-Rohr and H. W. Spiess, *Multidimensional Solid State NMR and Polymers* Academic Press, London, (1994).
71. E. Roessler, M. Taupitz, and H. M. Vieth, *Ber. Bunsengesellschaft* **93**, 1241 (1989).
72. T. Bernhard and U. Haeberlen, *Chem. Phys. Lett*. **186**, 307 (1991).
73. A. Detken, P. Focke, H. Zimmermann, U. Haeberlen, Z. Olejniczak, and Z. T. Lalowicz, *Z. Naturforsch*. **50a**, 95 (1995).
74. A. Detken and H. Zimmermann, *J. Chem. Phys*. **108**, 5845 (1998).
75. S. Clough, A. J. Horsewill, and M. N. J. Paley, *Phys. Rev. Lett*. **46**, 71 (1981).
76. S. Clough and A. J. Horsewill, *Phys. Rev*. B **25**, 4911 (1982).
77. S. Clough, A. J. Horsewill, P. J. Mcdonald, and F. O. Zelaya, *Phys. Rev. Lett*. **55**, 1794 (1985).

78. A. Heidemann, S. Clough, P. J. Mcdonald, A. J. Horsewill, and K. Neumaier, *Zeitschrift Fur Physik B-Condensed Matter* **58**, 141 (1985).
79. P. J. Mcdonald, G. J. Barker, S. Clough, R. M. Green, and A. J. Horsewill, *Mol. Phys.* **57**, 901 (1986).
80. A. J. Horsewill, A. M. Alsanoosi, and C. J. Carlile, *J. Phys. C-Solid State Phys.* **20**, L869 (1987).
81. Z. T. Lalowicz, M. Punkkinen, Z. Olejniczak, A. Birczytiski, and U. Haeberlen, *Solid State Nuclear Magnet. Reson.* **22**, 373 (2002).
82. Z. Olejniczak, Z. T. Lalowicz, T. Schmidt, H. Zimmermann, U. Haeberlen, and H. Schmitt, *J. Chem. Phys.* **116**, 10343 (2002).
83. T. Schmidt, H. Schmitt, U. Haeberlen, Z. Olejniczak, and Z. T. Lalowicz, *J. Chem. Phys.* **117**, 9818 (2002).
84. C. Cohen-Tannoudji, B. Diu, and F. Laloe, *Mechanique Quantique*, Hermann Editeurs, Paris, (1977).
85. S. Szymanski and P. Bernatowicz, *Ann. Rep. NMR Spectroscopy* **54,** 1 (2005).
86. R. B. Bell, *The Tunnel Efect in Chemistry*, Chapman & Hall, London & NY (1980).
87. A. Abragam, *Principles of Nuclear Magnetism*, Clarendon Press Oxford (1961).
88. C. P. Slichter, *Principles of Magnetic Resonance 3rd Edition*, Springer Verlag, Berlin, Heidelberg, New York (1990).
89. R. Ernst, G. Bodenhausen, and A. Wokaun, *Principles of NMR in One and Two Dimensions*, Clarendon Press, Oxford (1987).
90. P. Mansfield and P. G. Morris, *NMR Imaging in Biomedicine*, Academic Press, New York, (1982).
91. P. T. Callaghan, *Principles of Nuclear Magnetic Resonance Microscopy*, Clarendon Press, Oxford (1991).
92. R. Kimmich, *NMR Tomography Diffusometry Relaxometry*, Springer, Berlin, (1997).
93. M. Mehring, *High Resolution NMR Spectroscopy in Solids*, Springer Verlag, Berlin, Heidelberg, New York, (1983).
94. M. E. Rose, *Elementary Theory of Angular Momentum*, Wiley, New York, (1957).
95. T. Gullion and J. Schaefer, *J. Magn. Res.* **81**, 196 (1989).
96. A. E. Bennett, R. G. Griffin, and S. Vega, *Springer Series in NMR* **33**, 1 (1994).
97. W. A. King, X. L. Luo, B. L. Scott, G. J. Kubas, and K. W. Zilm, *J. Am. Chem. Soc.* **118**, 6782 (1996).
98. G. J. Kubas, J. E. Nelson, J. C. Bryan, J. Eckert, L. Wisniewski, and K. Zilm, *Inorg. Chem.* **33**, 2954 (1994).
99. G. Facey, D. Gusev, S. Macholl, R. H. Morris, and G. Buntkowsky, *Phys. Chem. Chem. Phys.* **2**, 935 (2000).
100. M. A. Esteruelas, F. J. Lahoz, E. Onate, L. A. Oro, C. Valero, and B. Zeier, *J. Am. Chem. Soc.* **117**, 7935 (1995).
101. R. H. Morris and R. J. Wittebort, *Mag. Res. Chem.* **35**, 243 (1997).
102. A. D. Bain, *Progess in NMR* **43**, 63 (2003).
103. V. I. Bakhmutov, *Magn. Reson. Chem.* **42**, 66 (2004).
104. H. W. Spiess, in *NMR Basic Principles and Progress*, P. Diehl, E. Fluck, and R. Kosfeld, (eds.), Springer Verlag, Berlin, **15**, 58 (1978).
105. S. Benz and U. Haeberlen, *J. Magn. Res.* **66**, 125 (1986).
106. A. Heuer and U. Haeberlen, *J. Chem. Phys.* **95**, 4201 (1991).
107. K. W. Zilm, R. A. Merill, M. W. Kummer, and G. J. Kubas, *J. Am. Chem. Soc.* **108**, 7837 (1986).
108. T. Pery, K. Pelzer, G. Buntkowsky, K. Philippot, H. H. Limbach, and B. Chaudret, *Chem. Phys. Chem.* **6**, 605 (2005).
109. J. Matthes, T. Pery, S. Gründemann, G. Buntkowsky, S. Sabo-Etienne, H. H. Limbach, and B. Chaudret, *J. Am. Chem. Soc.* **126**, 8366 (2004).
110. G. Buntkowsky, B. Walaszek, A. Adamczyk, Y. Xu, H.-H. Limbach, and B. Chaudret, *Phys. Chem. Chem. Phys.* **8**, 1929 (2006).